National Library of Canada
Acquisitions and Bibliographic Services Branch
395 Wellington Street
Ottawa, Ontario
K1A 0N4

Bibliothèque nationale du Canada
Direction des acquisitions et des services bibliographiques
395, rue Wellington
Ottawa (Ontario)
K1A 0N4

Your file Votre référence

Our file Notre référence

NOTICE

The quality of this microform is heavily dependent upon the quality of the original thesis submitted for microfilming. Every effort has been made to ensure the highest quality of reproduction possible.

If pages are missing, contact the university which granted the degree.

Some pages may have indistinct print especially if the original pages were typed with a poor typewriter ribbon or if the university sent us an inferior photocopy.

AVIS

La qualité de cette microforme dépend grandement de la qualité de la thèse soumise au microfilmage. Nous avons tout fait pour assurer une qualité supérieure de reproduction.

S'il manque des pages, veuillez communiquer avec l'université qui a conféré le grade.

La qualité d'impression de certaines pages peut laisser à désirer, surtout si les pages originales ont été dactylographiées à l'aide d'un ruban usé ou si l'université nous a fait parvenir une photocopie de qualité inférieure.

Canada

The Penetration of Electromagnetic Fields Through Open and Loaded Apertures

by

Christopher L. Gardner

A Thesis
Presented to the School of Graduate Studies and Research
of the University of Ottawa
in Partial Fulfillment of the
Requirements for the Degree of
Master of Applied Science
in
Electrical Engineering

Ottawa, Ontario, Canada, 1993

ISBN 0-315-89631-0

Canada

UNIVERSITÉ D'OTTAWA
UNIVERSITY OF OTTAWA

For Rosemary and

My Parents

I hereby declare that I am the sole author of this document. I authorize the University of Ottawa to lend this document to other institutions or individuals for the purpose of scholarly research.

Christopher L. Gardner

I further authorize the University of Ottawa to reproduce this document by photo-copying or by other means, in total or in part, at the request of other institutions or individuals for the purpose of scholarly research.

Christopher L. Gardner

Abstract

To ensure that an electronic system will work properly under all conditions, its designer must control the flow of electromagnetic (EM) fields to and from the system. The principal method of control is the use of a metallic enclosure or shield. In many cases, the effectiveness of the shield is determined, not by the bulk material properties, but by apertures that exist in the shield. These apertures may be introduced intentionally, as in the case of windows in the skin of an aircraft, or unintentionally, as in the case of an improperly welded seam or poorly gasketed door. To minimize the penetration of EM fields through a large aperture, the aperture is sometimes loaded with a conductive material.

Previous workers have shown that the penetration of EM fields through open or loaded apertures can be calculated by determining the equivalent magnetic surface currents, $\vec{M}_s$, that exist over the surface of the aperture. For small apertures, the equivalent magnetic and electric dipole moments (and polarizabilities) are related to the irrotational and solenoidal components of $\vec{M}_s$ respectively. In this thesis, the relevant integro-differential equations are solved using the Method of Moments to determine $\vec{M}_s$ and to calculate the equivalent polarizabilities and shielding effectiveness of a small, square aperture loaded with an impedance sheet.

Results of measurements of the penetration of EM fields through an aperture loaded with conductive material made using a dual transverse electromagnetic (TEM) cell over a frequency range of 2 to 200 MHz are presented and compared with the numerical results. The conductive materials examined include carbon, hybrid and non-carbon composite materials, and metallic grids and meshes. The composite samples were fabricated to study the effects of fibre orientation, conductivity, sample lay-up, and degree of hybridization on the electromagnetic shielding properties. Wire grids and meshes were fabricated to study the effect of wire spacing on shielding properties.

Acknowledgements

I would like to express my sincere gratitude to Dr. George Costache for his guidance throughout this work, and for sharing his knowledge of and enthusiasm for the field of electromagnetics with me.

This work was carried out while I was a full time employee at the Defence Research Establishment Ottawa (DREO) and would not have been completed without the moral and financial support of DREO management. I am particularly indebted to Dr. J.L. Pearce, Chief of DREO, to Mr. G. Marwood and Mr. W. Hindson, both Directors of the Electronics Division and to my Section Head, Dr. F. Szabo.

I have benefitted greatly from discussions I have had with my colleagues at DREO. Dr. Satish Kashyap suggested the use of the dual TEM cell method and has shared his knowledge of the subject with me. Mr. Miles Burton has been a constant source of useful information in the field of electromagnetics. Only once did I ask a question that Miles couldn't answer! Mr. Joe Seregelyi has provided advice on the experimental aspects of this work and Mr. Marc Dion has answered all of my computer related questions. The fabrication of the composite samples was made possible through interaction with Dr. Ken Street (formerly) of the Defence Research Establishment Pacific (DREP). I am indebted to Ken for sharing some of his vast knowledge of composite materials with me.

I would like to thank Mr. R. Apps and Mr. S. McCullough for their assistance with some of the measurements, and to Mr. E. Jensen for producing the laminates.

Table of Contents

Table of Figures

Table of Tables

Chapter 1:

Introduction

The electromagnetic (EM) vulnerability of electronic systems such as computers, medical devices, aircraft control systems and communication systems is of concern. Potential electromagnetic threats to electronics include natural sources, such as lightning and electrostatic discharge, as well as a variety of man-made sources, including the intense electromagnetic pulse from a high altitude nuclear explosion [1], high power microwave weapons [2], and the "normal" EM environment produced by high power radars, radio and TV transmitters, and unwanted RF emissions from the operation of a broad range of electronic devices. The proliferation of electronic devices is resulting in an electromagnetic environment that is becoming increasingly more severe.

At the same time, technological advances such as the use of plastics and composite materials for construction; increased clock speeds in digital equipment; and miniaturization of electronics are resulting in increased EM susceptibility of many electronic systems as more electronic circuits are crowded into less space.

To ensure that their electronic systems work properly under all operating conditions, designers must ensure that their systems are compatible with the EM environment. One of the principal methods used to control the propagation of EM fields either into or out of an equipment compartment is the use of a metallic shield [3]. Using a solid metallic shield, a shielding effectiveness of

90 dB or more is easy to obtain for all EM fields with the exception of low frequency magnetic fields. In most cases, however, the effectiveness of the metallic (conductive) shield is not determined by the bulk material properties of the shield but rather by apertures that exist in the shield. These apertures may be introduced intentionally as in the case of windows in the skin of an aircraft or unintentionally as in the case of improperly welded seams, poorly gasketed doors and so on. To minimize the penetration of EM fields through apertures, the aperture is sometimes covered or "loaded" with a conductive material. The use of a conductive screen to minimize penetration through a window while maintaining adequate visibility is a typical example of aperture loading.

A knowledge of the penetration of EM fields through open and loaded apertures of various shapes and sizes is important to ensure that equipment is electromagnetically compatible with its environment. The objectives of this work were, firstly, to measure the penetration of electric and magnetic fields through an aperture loaded with conductive materials and, secondly, to compare these results with values calculated from small aperture theory using the Method of Moments.

Chapter 2:
Theoretical Background

2.1 Definition of the Problem

The problem being considered is the penetration of the electromagnetic field produced by electric and magnetic sources, $\vec{J}_i$ and $\vec{M}_i$, through an aperture, A, in an infinite planar screen as shown in Figure 1. The screen, S, is assumed to be perfectly conducting and vanishingly thin. It is located in a homogeneous medium characterised by constitutive parameters μ, ϵ. The aperture may or may not be loaded with a conductive sheet defined [12] by a sheet impedance dyad, $\overleftrightarrow{Z}_s$, which relates the current flow, $\vec{J}_s$, through the sheet to the tangential electric field, $\vec{E}_t$, in the aperture.

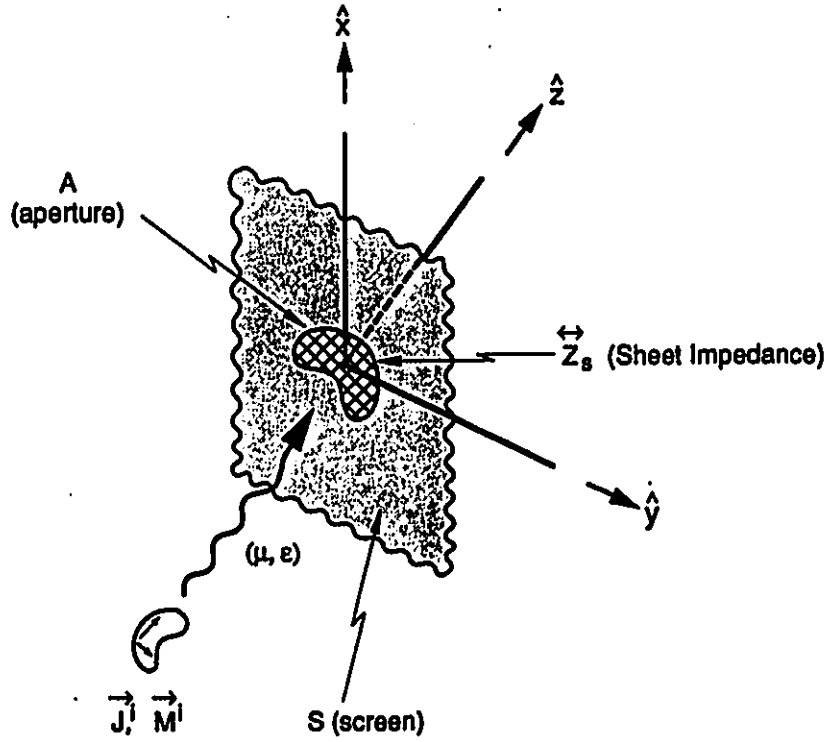

Figure 1 - The Penetration of Electromagnetic Fields Through an Aperture

2.2 Equivalence Principle

The aperture problem outlined above is most conveniently treated using the equivalence principle [4]. A given field distribution on the right hand side (z positive) of the screen S can result from a variety of source distributions on the left hand side of the screen. Two source distributions that give rise to the same fields are said to be *equivalent.* Using this principle, the aperture problem can be dealt with by considering the screen to be continuous and by placing appropriate magnetic surface currents $\vec{M}_s$ over the aperture as shown in Figure 2.

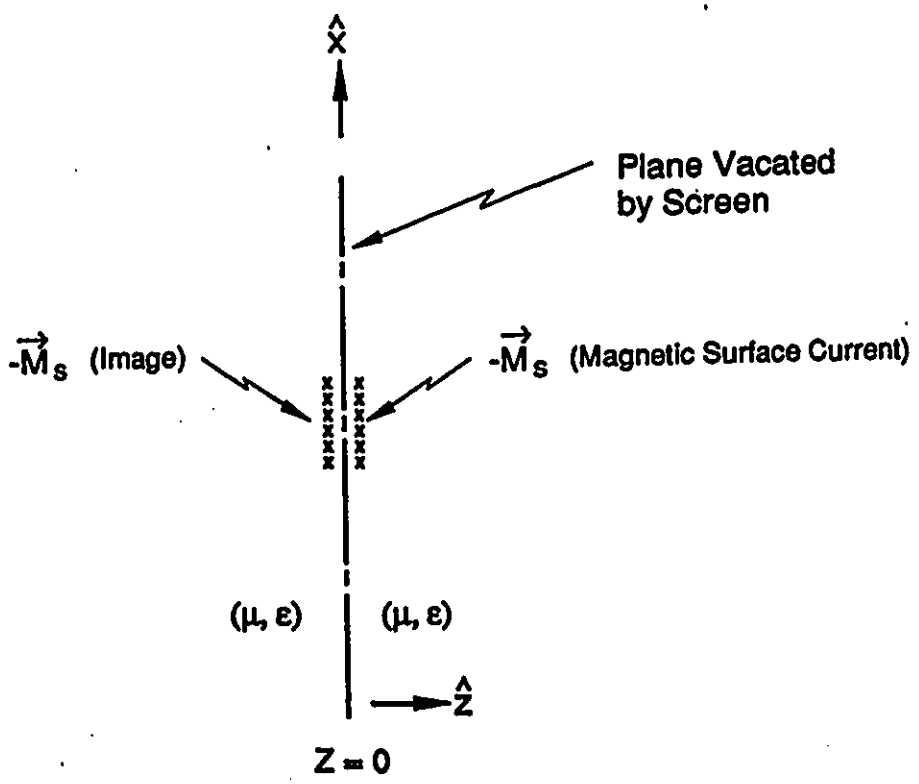

Figure 2 - The Equivalent Source Distribution for the Shadow Side of the Aperture

Using this approach, the magnetic field ($\vec{H}^-$) on the left (illuminated) side can be written [5] as

$$\vec{H}^-(\vec{r}) = \vec{H}^{sc} - \frac{j\omega}{k^2}[k^2\vec{F}(\vec{r}) + \nabla(\nabla\cdot\vec{F}(\vec{r}))]. \tag{1}$$

In this expression $\vec{F}(\vec{r})$ is the electric vector potential given by

$$\vec{F}(\vec{r}) = \frac{e}{4\pi}\int_A\int 2\vec{M}_s(\vec{r})G(\vec{r},\vec{r}')ds' \tag{2}$$

where

$$\vec{M}_s(\vec{r}) = \hat{z} \times \vec{E}_t \tag{3}$$

and

$$G(\vec{r},\vec{r}') = \frac{e^{-jk|\vec{r}-\vec{r}'|}}{|\vec{r}-\vec{r}'|}. \tag{4}$$

$\vec{H}^{sc}$ is the short circuit magnetic field [5], k is the propagation constant and ω is the angular frequency.

For the right hand side of the screen , the magnetic field, $\vec{H}^+$, is given by,

$$\vec{H}^+(\vec{r}) = \frac{j\omega}{k^2}[k^2\vec{F}(\vec{r}) + \nabla(\nabla\cdot\vec{F}(\vec{r}))]. \tag{5}$$

The electric fields in the two half spaces are given by the relationships,

$$\vec{E}^-(\vec{r}) = \vec{E}^{sc} - \frac{1}{e}\nabla\times\vec{F}(\vec{r}) \tag{6}$$

and

$$\vec{E}^{s}(\vec{r}) = \frac{1}{e}\nabla\times\vec{F}(\vec{r}) \ . \tag{7}$$

In this expression $\vec{E}^{sc}$ is the short circuit electric field [5].

From the above equations it is seen that if the equivalent magnetic currents, $\vec{M}_s$, can be found, then the penetration of EM fields through the aperture can be determined. In the next sections, methods of calculating $\vec{M}_s$ for open and loaded apertures are discussed.

2.3 Small Aperture Theory

If the magnetic surface current density in the aperture A is $\vec{M}_s$ then, for A small and r remote from the source region, the electromagnetic field due to this magnetic source can be approximated [6] by the radiation from a magnetic dipole moment, $\vec{p}_m$, and an electric dipole moment, $\vec{p}_e$, both located at the centre of A. These dipole moments are related [6] to the magnetic current, $\vec{M}_s$, by the expressions

$$\vec{p}_e = -\frac{\epsilon}{2}\int_A\int \vec{r}'\times\vec{M}_s(\vec{r}')ds' \tag{8}$$

and

$$\vec{p}_m = \frac{1}{\mu}\int_A\int \vec{r}' m_s(\vec{r}')ds' = -\frac{1}{\omega\mu}\int_A\int \vec{M}_s(\vec{r}')ds' \ . \tag{9}$$

In equation (9), m_s, the magnetic charge density, is defined from the equation of continuity by [4]

$$m_s = \frac{1}{\omega}\nabla_t \cdot \vec{M}_s \,. \tag{10}$$

In deriving (9) the following identity [7] has been used.

$$\int\int_A \vec{r}'\nabla_t \cdot \vec{M}_s(\vec{r}')ds' = \int\int_A \vec{M}_s(\vec{r}')ds' \,. \tag{11}$$

From the relationships for $\vec{p}_e$ and $\vec{p}_m$ given above, it can be shown that the magnetic dipole moment is related to the irrotational component of $\vec{M}_s$ and that the electric dipole moment is related to the solenoidal component of $\vec{M}_s$.

The equivalent dipole moments, $\vec{p}_e$ and $\vec{p}_m$, are proportional to the incident field strengths E_z^i and $\vec{H}_t^i$ and electric and magnetic polarizabilities, α_e and $\bar{\bar{\alpha}}_m$, can be defined by

$$\vec{p}_e = e\alpha_e E_z^i \tag{12}$$

and

$$\vec{p}_m = \bar{\bar{\alpha}}_m \cdot \vec{H}_t^i \,. \tag{13}$$

In these expressions, E_z^i is the normal component of the incident electric field and $\vec{H}_t^i$ is the tangential component of the incident magnetic field.

For a small open circular aperture of radius a, the polarizabilities are known [8] to be

$$\alpha_e = -\frac{a^3}{3} \tag{14}$$

and

$$\alpha_{mx,my} = -\frac{2a^3}{3} . \tag{15}$$

where $\alpha_{mx,my}$ are the principal components of $\ddot{\alpha}_m$.

2.4 Penetration of EM Fields Through Open Apertures

2.4.1 Boundary Conditions

(i) On the Screen: At the surface of the metallic screen both $\vec{E}_t$ and $\vec{H}_n$ are zero.

(ii) In the Aperture: $\vec{E}$ and $\vec{H}$ are continuous.

(iii) At the Edge: $\vec{E}_t$ falls to zero as $\sqrt{s}$. This implies $\hat{n}\cdot\vec{M}_s = 0$ at the screen edge. $\hat{n}$ is normal to the edge of the screen. $\vec{H}_t$ goes to infinity as $1/\sqrt{s}$.

In the above expressions s is the distance from the edge of the aperture.

2.4.2 Derivation of Basic Equations

When the aperture is open, the transverse components of the magnetic fields are continuous and the following relationship can be written [5]

$$\lim_{z\to 0}(\vec{H}^{-}(\vec{r})\times \hat{z}) = \lim_{z\to 0}(\vec{H}^{+}(\vec{r})\times \hat{z}) \tag{16}$$

which from equations (1) and (5) leads to the relationship

$$\vec{H}^{sc}\times \hat{z} = \frac{2j\omega}{k^2}[\nabla_t\nabla_t\cdot\vec{F}(\vec{r})+k^2\vec{F}(\vec{r})]\times \hat{z} \tag{17}$$

but

$$\vec{H}^{sc}\times \hat{z} = 2\vec{H}^{i}\times \hat{z} \tag{18}$$

thus

$$\vec{H}^{i}\times \hat{z} = \frac{j\omega}{k^2}[\nabla_t\nabla_t\cdot\vec{F}(\vec{r})+k^2\vec{F}(\vec{r})] \times \hat{z}\ . \tag{19}$$

The magnetic surface current, $\vec{M}_s$, can then be determined if equation (19) can be solved.

Once $\vec{M}_s$ is known, the electric field in the two half spaces can be calculated from (6) and (7).

Imposing continuity of the normal component of the electric field in the aperture leads to the relationship

$$\hat{z}\cdot\vec{E}^{i} = \frac{1}{\epsilon}(\nabla\times\vec{F}(\vec{r}))\cdot \hat{z}\ . \tag{20}$$

From equation (20), it is seen that the solution of the equation obtained from equating the normal component of the electric field only gives the rotational component of $\vec{F}$ (and $\vec{M}_s$). It should also be noted that, if there is a non-zero E_x^i in the aperture (ie. for a plane wave, whenever the direction of propagation is not normal to the aperture surface), then $\vec{M}_s$ has a solenoidal component.

From the expressions above it can be seen that, provided $\vec{H}^i$ is completely defined in the aperture (ie magnitude and phase over the entire aperture), (19) provides a complete solution to $\vec{M}_s$.

Since $\vec{F}$ is two dimensional, being defined only on the surface of the aperture, (ie $\vec{F}=\hat{x}F_x+\hat{y}F_y$) (19) can be written in the form

$$\vec{H}_t^i = \frac{j\omega}{k^2}[\nabla_t\nabla_t\cdot\vec{F}(\vec{r})+k^2\vec{F}(\vec{r})] \tag{21}$$

where

$$\vec{H}_t = \hat{x}H_x+\hat{y}H_y \ . \tag{22}$$

If we turn our attention to the particular case of the fields in a TEM cell, which is discussed in later sections, then the incident magnetic field, $\vec{H}_c^i$, can be written [9] in the particularly simple form

$$\vec{H}_t^i = \hat{y}\ H_0 e^{-jkx} \tag{23}$$

where the x-axis is the direction of propagation of the plane wave through the TEM cell and the y-axis lies in the plane of the TEM cell plenum.

Noting that the electric vector potential, $\vec{F}$, can be written as the sum of an irrotational component, $\vec{F}_I$ (*where* $\nabla_t \times \vec{F}_I = 0$), and a solenoidal or rotational component, $\vec{F}_R$ (*where* $\nabla_t \times \vec{F}_R \neq 0$), then equations for $\vec{F}_I$ and $\vec{F}_R$ are obtained in the following way.

Taking the curl of both sides of (21) gives the following relationship

$$j\omega \nabla_t \times \vec{F}_R = \nabla_t \times \vec{H}_t^i = -jkH_0 e^{-jkx} = -jkH_0 \ . \tag{24}$$

Since $\vec{M}_a$ only has a y-component (ie. $\vec{M}_a$ *and* $\vec{H}_t^i$ are collinear), equation (24) can be written

$$j\omega \frac{\partial F_y}{\partial x} = -jkH_0 \ . \tag{25}$$

Integration of (25) then yields

$$j\omega F_y = -jkH_0 x \ . \tag{26}$$

The following equation for the irrotational component of $\vec{F}$ is obtained by equating the irrotational components on each side of (21)

$$\frac{j\omega}{k^2}[\nabla_t \nabla_t \cdot \vec{F}_I + k^2 \vec{F}_I] = \vec{H}_{t,I}^i \tag{27}$$

where $\vec{H}_{t,I}^i$ is the irrotational component of incident magnetic field.

For small apertures, the second term on the left hand side of (27) (ie the term in k^2) can be neglected and the solution for the irrotational component is approximately given by the equation

$$\frac{j\omega}{k^2}[\nabla_t \nabla_t \cdot \vec{F}_I] - \vec{H}^I_{t,I} \,. \tag{28}$$

Since $\nabla \cdot \vec{F}_R = 0$, the first term on the left hand side of equation (21) does not contribute to the determination of $\vec{F}_R$. In addition, from Maxwell's curl equations, we can write

$$\hat{z} \cdot \vec{E}^I - \frac{1}{j\omega\epsilon} \hat{z} \cdot \nabla \times \vec{H}^I - \frac{1}{j\omega\epsilon}\left[\frac{\partial H_x}{\partial y} - \frac{\partial H_y}{\partial x}\right] \tag{29}$$

and it is seen that the normal component of the electric field is properly defined provided that $\vec{H}_t$ is completely defined and that equation (26), which is included as part of the solution of (21), is equivalent to (20).

The following section shows that the equations derived above are identical with those derived by a Rayleigh (low frequency) expansion [5,10] of (21). The method of subdivision of the vector quantities into irrotational and solenoidal components has been used because this method appears to provide easier solution of the loaded aperture equations.

2.4.3 Rayleigh Expansion (Low Frequency Approximation)

Stevenson [10] and van Bladel [5] have shown that, at low frequencies, the field and potential quantities can be expanded in terms of the small parameter jk. For example

$$\vec{F} = \vec{F}_0 + jk\vec{F}_1 + \cdots \tag{30}$$

and

$$\vec{E} = \vec{E}_0 + jk\vec{E}_1 + \cdots = \frac{1}{\epsilon}\nabla\times\vec{F}_0 + \frac{jk}{\epsilon}\nabla\times\vec{F}_1 + \cdots \tag{31}$$

and

$$\vec{H}_t = \vec{H}_{t,0} + jk\vec{H}_{t,1} + \cdots . \tag{32}$$

If these expansions are inserted into the aperture equations derived earlier (equations (19) and (20) for an open aperture) and terms of the same order in jk are equated then an appropriate set of equations is obtained for the determination of the n^{th} - order components of $\vec{F}$.

Substitution of the expansions for $\vec{F}$ and $\vec{H}_t$ into (21) yields

$$\nabla_t\nabla_t\cdot(\vec{F}_0+jk\vec{F}_1+\cdots) - (jk)^2(\vec{F}_0+jk\vec{F}_1+\cdots) = -\frac{jk}{c}(\vec{H}_{t,0}+jk\vec{H}_{t,1}+\cdots) . \tag{33}$$

Equating terms in equal powers of $(jk)^n$ yields;

For n=0

$$\nabla_t\nabla_t\cdot\vec{F}_0 = 0 . \tag{34}$$

This shows that $\vec{F}_0$ is the leading term of the solenoidal component of $\vec{F}$.

For n=1

$$\nabla_t\nabla_t\cdot\vec{F}_1 = -\frac{\vec{H}_{t,0}}{c} . \tag{35}$$

This shows that $\vec{F}_1$ is the leading term of the irrotational component of $\vec{F}$. This equation is equivalent to (28).

For n = 2

$$\nabla_t \nabla_t \cdot \vec{F}_2 - \vec{F}_0 = -\frac{\vec{H}_{t,1}}{c} . \tag{36}$$

Since $\vec{H}_{t,1}$ is solenoidal, it follows that $\nabla_t \nabla_t \cdot \vec{F}_2 = 0$ and the above equation reduces to

$$\vec{F}_0 = \frac{\vec{H}_{t,1}}{c} . \tag{37}$$

In the above equations c is the speed of light. Equation (37) is equivalent to equation (26). This analysis shows that the equations derived using Rayleigh expansion are the same as those obtained by decomposition of the vector components into irrotational and solenoidal components. In particular, the zeroth order component of $\vec{F}$ is rotational and the first order component is irrotational. Expansion by either method leads to identical equations when the aperture is small.

2.5 Penetration of EM Fields Through Loaded Apertures

2.5.1 Boundary Conditions

(i) On the Screen: At the surface of the metallic screen both $\vec{E}_t$ and $\vec{H}_n$ are zero.

(ii) In the Aperture: $\vec{E}_t$ and $\vec{H}_n$ are continuous. The tangential magnetic fields and normal electric fields are related to the surface current and charge by the relationships.

$$(\vec{H}^+ - \vec{H}^-) \times \hat{z} = \vec{J}_s \quad \text{and} \quad \hat{z} \cdot (\vec{E}^+ - \vec{E}^-) = \rho_s .$$

(iii) At the Edge: $\vec{E}_t$ falls to zero as $\sqrt{s}$. This implies $\hat{n} \cdot \vec{M}_s = 0$ at the screen edge.
$\vec{H}_t$ goes to infinity as $1/\sqrt{s}$.

2.5.2 Derivation of Basic Equations

When the aperture is loaded with an impedance sheet defined in terms of a surface impedance dyadic, $\vec{\vec{Z}}_s$, the tangential component of the magnetic field is no longer continuous. In this case the appropriate boundary condition [11] is

$$[\vec{H}^+(\vec{r}) - \vec{H}^-(\vec{r})] \times \hat{z} = \vec{J}_s . \tag{38}$$

The electric surface current, $\vec{J}_s$, and the magnetic surface current, $\vec{M}_s$, are related to the tangential electric field in the aperture through the relationships

$$\vec{E}_t = \vec{\vec{Z}}_s \cdot \vec{J}_s \tag{39}$$

and

$$\vec{M}_s = \hat{z}\times\vec{E}_t \ . \tag{40}$$

Depending on the properties of the material that is used to load (or cover) the aperture, the dyad, $\vec{\vec{Z}}_s$, can have a number of forms.

In the following sections, several forms of $\vec{\vec{Z}}_s$ corresponding to shielding materials of practical interest are considered and the corresponding integro-differential equations are derived.

2.5.2.1 An Isotropic Resistive Sheet

Many materials used to provide shielding to apertures can be considered as isotropic, resistive sheets. One example is the deposition of a transparent conductive coating onto various optical substrates such as plastic or glass. Materials prepared in this manner can provide good EM shielding without seriously degrading optical transparency. Carbon composites can also be made effectively isotropic by using lay-ups that have fibres running in a number of orientations (eg 0°, ±45°, 90°).

For a thin, homogeneous material of conductivity, σ, and thickness, d, the surface impedance, Z_s, is scalar and can be expressed in terms of a surface resistivity, R_s, given by

$$R_s = \frac{1}{\sigma d} \tag{41}$$

or ,equivalently, in terms of a surface conductivity, $\sigma_s = 1/R_s$.

In this case, $\vec{J}_s$ is related to the tangential electric field through the relationship

$$\vec{J}_s = \sigma_s \vec{E}_t \ . \qquad (42)$$

Substituting the expressions for $\vec{H}^+$ and $\vec{H}^-$ (equations (1) and (5)) as well as the results given in equations (40) and (42) into (38) yields the following integro-differential equation

$$\frac{j\omega}{k^2}\left[\nabla_t \nabla_t \cdot \vec{F}(\vec{r}) + k^2 \vec{F}(\vec{r})\right] + \frac{\sigma_s}{2}\vec{M}_s = \vec{H}_t^i \ . \qquad (43)$$

If $\vec{F}$ is expressed, as before, as a sum of irrotational and rotational components the following pair of equations is obtained for $\vec{F}_I$ and $\vec{F}_R$.

$$\frac{j\omega}{k^2}\left[\nabla_t \nabla_t \cdot \vec{F}_I + k^2 \vec{F}_I\right] + \frac{\sigma_s}{2}\vec{M}_{s,I} = \vec{H}_{t,I}^i \qquad (44)$$

and

$$j\omega F_R^y + \frac{\sigma_s}{2} M_{s,R}^y = -jkH_0 x \ . \qquad (45)$$

2.5.2.2 An Anisotropic Resistive Sheet

If we consider a material consisting of uni-directional conductive fibres (with no electrical contact between the neighbouring fibres) then the flow of current is only along the fibre direction and the conductivity of the material is anisotropic. This is a good approximation of the carbon composite materials having uni-directional lay-up that were measured in the experimental portion of this work.

If the resistance of a unit length of a single fibre is R and the number of fibres per unit length is n, then the surface resistivity of the sample is given by

$$R_s = \frac{R}{n} \tag{46}$$

since all of the fibres are connected electrically in parallel.

If we choose the x-axis to lie along the direction of the fibres, then, in this coordinate system, the impedance dyadic, $\bar{\bar{Z}}_s$, becomes simply

$$\bar{\bar{Z}}_s = \hat{x}\hat{x}\, R_s \ . \tag{47}$$

Substitution of (47) into (39) then yields the following equation

$$\frac{j\omega}{k^2}[\nabla_t\nabla_t\cdot\vec{F}(\vec{r})+k^2\vec{F}(\vec{r})]+\hat{y}\left(\frac{1}{2R_s}\right)M_s^y = \vec{H}_t^i \ . \tag{48}$$

If $\vec{F}$ is expressed as a sum of irrotational and solenoidal (rotational) components, the following pair of equations are obtained for $\vec{F}_I$ and $\vec{F}_R$.

$$\frac{j\omega}{k^2}[\nabla_t\nabla_t\cdot\vec{F}_I(\vec{r})+k^2\vec{F}_I(\vec{r})]+\hat{y}\left(\frac{1}{2R_s}\right)M_{s,I}^y = \vec{H}_{t,I}^i \tag{49}$$

and

$$j\omega F_R^y+\left(\frac{1}{2R_s}\right)M_{s,R}^y = -jkH_0x \ . \tag{50}$$

2.5.2.3 A Bonded Wire Mesh

1. The Equivalent Sheet Impedance

To derive the basic equations for the case of a bonded wire mesh, some of the results derived previously by Casey [12] have been used. In the derivation of the equations I assume, as Casey did, that the aperture is small and that a low frequency (quasi-static) approximation can be used.

Kontorovich [13] has shown that the electromagnetic properties of a bonded wire mesh can be described in terms of an equivalent sheet impedance operator when the mesh size is small compared with the wavelength. Using this approach, the tangential electric field, $\vec{E}_t$, in the aperture is given by

$$\vec{E}_t = \vec{\vec{Z}}_s \cdot \vec{J}_s \tag{51}$$

where $\vec{\vec{Z}}_s$ is a dyadic operator that relates the space averaged tangential electric field to the space averaged surface current, $\vec{J}_s$.

When the meshes are square, with mesh size a_s, and the mesh wires are electrically bonded, then Casey [12] has shown that

$$\vec{\vec{Z}}_s = (Z_w a_s + j\omega L_s)(\vec{\vec{I}} - \hat{n}\hat{n}) - \frac{a_s^2}{j\omega C_s}\nabla_s\nabla_s \,. \tag{52}$$

The parameters Z_w, L_s and C_s represent the internal impedance of the wire and the external inductance and capacitance of the mesh respectively. These parameters are given by

$$L_s = \frac{\mu_0 a_s}{2\pi} \ln\left(1 - e^{\frac{-2\pi r_w}{a_s}}\right)^{-1} \tag{53}$$

$$\frac{1}{C_s} = \frac{1}{4\pi\epsilon_0 a_s} \ln\left(1 - e^{\frac{-2\pi r_w}{a_s}}\right)^{-1} \tag{54}$$

$$Z_w = \frac{R_w \sqrt{j\omega\tau_w}\, I_0\left(\sqrt{j\omega\tau_w}\right)}{2 I_1\left(\sqrt{j\omega\tau_w}\right)} \tag{55}$$

where r_w is the wire radius, τ_w is the diffusion time constant, and I_0 and I_1 are Bessel functions of the first kind and R_w is the dc resistance of the wire per unit length. Using the expressions given by Casey [12] for R_w and τ_w, it can be shown that the contribution of the internal impedance of the wires to the impedance of the wire grid is negligible over the frequency range of 2-500 MHz discussed in this report.

Equation (51) can then be rewritten in the form

$$\vec{E}_t = j\omega L_s \vec{J}_s + \frac{a_s^2}{C_s} \nabla_s \rho_s \,. \tag{56}$$

In this equation, ρ_s is the space averaged surface electric charge density of the mesh.

The derivation of (56) uses the equation of continuity

$$\nabla_s \cdot J_s + j\omega\rho_s = 0 \,. \tag{57}$$

Equation (56) shows that the magnitude of the tangential electric field in the aperture has two components. The first term on the right hand side of (56) can be thought of as arising from the flow of current along the wires of the screen with the magnitude of the current being controlled by the external inductance of the screen. The second term represents the contribution to $\vec{E}_t$ that results from the build up of charge on the wires with the magnitude of the surface charge being related to the capacitance of the grid. Using the static relationship that

$$\rho = C V \tag{58}$$

then, by taking the gradient of both sides, it can be shown that the contribution of the surface charge to the tangential electric field is given by

$$\vec{E}_t = \frac{a_s^2}{C_s} \nabla_s \rho_s \, . \tag{59}$$

For a system of parallel conductors (ie. a uni-directional wire grid), the external inductance and capacitance of the screen are related by the relationship that $C_s = 1/c^2 L_s$ [14]. Comparison with the expressions for L_s and C_s given in equations (53) and (54) shows that the capacitance for the bonded wire mesh is one half that predicted by the above expression. The second set of orthogonal wires effectively reduces the capacitance by a factor of two (ie the two sets of wires are connected in parallel).

If $r_w << a_s$, then, by expanding the exponential term, L_s can be rewritten in the form

$$L_s = \frac{\mu_0 a_s}{2\pi} [\ln(a_s/r_w) - 1.84] \, . \tag{60}$$

Substitution of (60) into (56) gives an expression for $\vec{E}_t$ in the form given by Kontorovich [13] and Wait [15].

2. Derivation of the Equation for the Irrotational Component of $\vec{M}_s$

Section 2.3 shows that the effective magnetic dipole of the aperture is related to the irrotational component of $\vec{M}_s$. Applying the quasi-static approximation to the case of a stationary magnetic field, the equation of continuity reduces to

$$\nabla_s \cdot \vec{J}_s = 0 \tag{61}$$

and equation (56) becomes

$$\vec{E}_t = j\omega L_s \vec{J}_s \,. \tag{62}$$

The appropriate equation for the calculation of $\vec{M}_{s,I}$ can then be obtained following the procedure of section 2.5.2.1 for an isotropic resistive sheet to give

$$\frac{j\omega}{k^2}[\nabla_s \nabla_s \cdot \vec{F}_I + k^2 \vec{F}_I] + \frac{1}{2\omega L_s}\vec{M}_{s,I} = \vec{H}^i_{t,0} \tag{63}$$

This equation is identical in form to (44). In this case the inductive reactance of the screen, $j\omega L_s$, replaces the surface resistivity, R_s. (63) shows that the magnetic insertion loss of the bonded wire grid will be frequency independent. This is the behaviour that is observed experimentally (see section 5.3).

3. Derivation of the Equation for the Solenoidal Component of $\vec{M}_s$

In the electrostatic limit there is no current flow and we can write [12]

$$\vec{E}_t = \frac{a_s^2}{C_s}\nabla_s\rho_s = \frac{a_s^2}{j\omega C_s}\nabla_s\nabla_s\cdot\vec{J}_s \,. \tag{64}$$

Attempts I made to formulate an analytical equation that would allow the calculation of the solenoidal component of $\vec{M}_s$ for the case of a bonded wire mesh were unsuccessful. However use of the general boundary condition (38) for an aperture loaded with an impedance sheet together with (64) which relates $\vec{E}_t$ and $\vec{J}_s$ provides a system of equations that can be solved numerically as is shown in Chapter 4. The same procedure can be used for a unidirectional wire screen or an unbonded wire mesh.

2.5.2.4 A Unidirectional Wire Screen

For the purposes of this discussion, I assume that the wires of the screen are oriented so that they lie along the x-axis.

1. Equivalent Sheet Impedance

Using the averaged boundary condition method, Kontorovich [16] has shown that tangential electric field in the aperture can be written

$$E_x = j\omega L_s[J_x + \frac{1}{k^2}\frac{\partial^2 J_x}{\partial x^2}] \tag{65}$$

where L_s is given by equation (53).

The similarity of equation (65) with the equation derived for a bonded wire mesh is obvious.

2. Derivation of the Equation for the Irrotational Component of $\vec{M}_s$

If the quasi-static approximation is applied to the magnetic field, then equation (65) reduces to $\vec{E}_t = \hat{x} j\omega L_s J_x$.

The appropriate equation for the calculation of $\vec{M}_{s,I}$ then becomes

$$\frac{j\omega}{k^2}[\nabla_s \nabla_s \cdot \vec{F}_I + k^2 \vec{F}_I] + \hat{y} \frac{1}{2\omega L_s} M^y_{s,I} = \vec{H}^i_{t,o} \ . \qquad (66)$$

2.5.2.5 An Unbonded Wire Mesh

1. Equivalent Sheet Impedance

The following expressions have also been given by Kontorovich [13] for the components of the tangential electric field for an unbonded wire mesh.

$$E_x = j\omega L_s [\, J_x + \frac{1}{2k^2} \frac{\partial^2 J_x}{\partial x^2} \,] \qquad (67)$$

and

$$E_y - j\omega L_s [\, J_y + \frac{1}{2k^2} \frac{\partial^2 J_y}{\partial y^2} \,] \,. \qquad (68)$$

2. Derivation of the Equation for the Irrotational Component of $\vec{M}_s$

Using the same procedure as in section 2.5.2.3, the basic equation for the bonded and unbonded meshes are found to be the same and equation (63) should be used.

Chapter 3:
An Overview of Previous Work

3.1 Introduction

The literature dealing with the penetration of electromagnetic fields through apertures is extensive. Aspects covered include subjects such as EM penetration through small and large apertures, through multiple apertures, cavity backed apertures and excitation of objects located behind an aperture in a screen. A good review of these subjects is given in the review paper of Butler, Rahmat-Samii and Mittra [6]. Discussion in this section of the thesis is restricted to the penetration of time-harmonic EM fields through a single aperture in a thin, planar and perfectly conducting screen of infinite extent. In most cases discussed, the aperture is also assumed to be electrically small. That is the aperture has dimensions small compared to the wavelength of the incident field.

3.2 EM Penetration Through Open Apertures

3.2.1 Analytical Solution for a Small, Circular Aperture

The theory of the penetration of EM fields through circular apertures was presented many years ago in the classical work of Bouwkamp [17,18] and Bethe [19]. Analytical solutions for EM penetration through apertures are only available for the special cases of circular apertures and elliptical apertures. More complicated geometries of practical interest, such as square and rectangular apertures can be solved numerically as discussed in later sections of this Chapter.

In his work, Bethe [19] demonstrated that the field radiated by a small aperture can be described in terms of a combination of equivalent electric ($\vec{p}_e$) and magnetic ($\vec{p}_m$) dipoles located at the centre of the aperture. The penetration of EM fields through a small aperture is illustrated qualitatively in Figure 3.

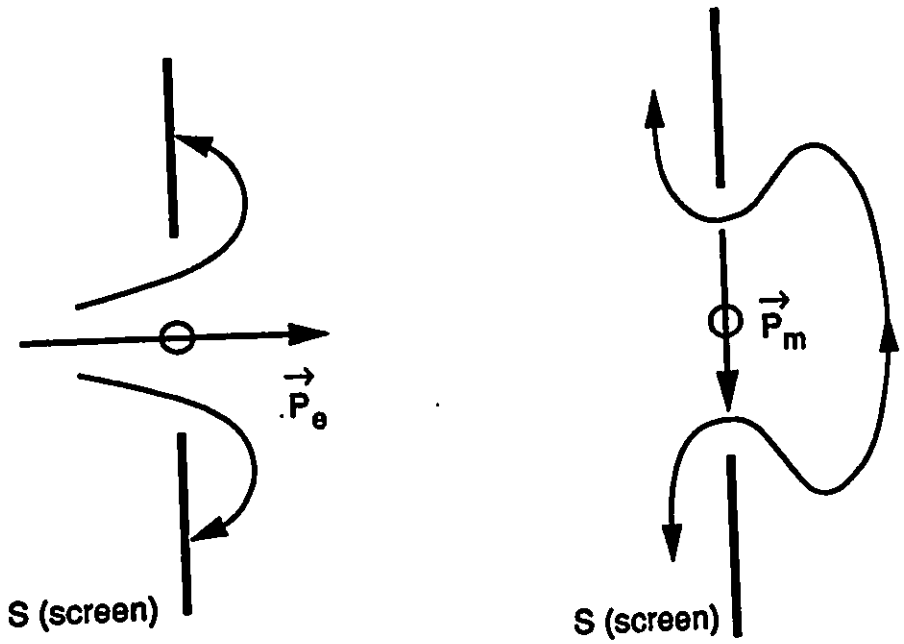

Figure 3 - Equivalent Dipole Representation of a Small Aperture

The equivalent dipole moments, $\vec{p}_e$ and $\vec{p}_m$, are proportional [7] to the incident field strengths E_z^i and $\vec{H}_t^i$ and electric and magnetic polarizabilities can be defined by the relationships

$$p_e = e\alpha_e E_z^i \tag{69}$$

and

$$\vec{p}_m = \bar{\bar{\alpha}} \cdot \vec{H}_t^i \,. \tag{70}$$

For a small, open and circular aperture of radius, a, the polarizabilities are known [8] to be

$$\alpha_e = -\frac{a^3}{3} \tag{71}$$

and

$$\alpha_m = -\frac{2a^3}{3} \,. \tag{72}$$

Polarizabilities for small apertures of other shapes have been measured by Cohn [20,21]. Shapes that Cohn has studied include the square, the rectangle, the rectangle with half circular ends, the rosette, the dumbbell , the H-shaped aperture and the cross with half-circular ends.

3.2.2 Solution of Aperture Equations Using Low Frequency (Rayleigh) Expansion

In section 2.4.3, simplification of the aperture equations by expansion of the field and potential in terms of the small parameter, jk, as proposed by Stevenson [10] was discussed. Van Bladel and coworkers [5,22] have solved the open aperture problem for a number of aperture shapes by adopting this low frequency expansion procedure and by expressing the magnetic surface current, $\vec{M}_s$, in terms of two unknown scalar potentials, Γ and Θ, as follows

$$\vec{M}_s = \nabla_t \Gamma + \hat{z} \times \nabla_t \Theta \,. \tag{73}$$

Using this approach, van Bladel and Butler [5] determined the equivalent electric and magnetic polarizabilities as follows.

3.2.2.1 Calculation of the Equivalent Electric Polarizability

$$\nabla_t^2 \frac{1}{2\pi} \iint_A \frac{\Theta_0}{|\vec{r} - \vec{r}'|} ds' = \hat{z} \cdot \vec{E}_0^i \tag{74}$$

with $\Theta_0 = 0$ on the aperture edge. In terms of the normalised parameter, τ_0, (74) reduces [5] to

$$\nabla_t^2 \frac{1}{2\pi} \iint_A \frac{\tau_0}{|\vec{r} - \vec{r}'|} ds' = \frac{1}{\sqrt{S}} \tag{75}$$

where S is the surface area of the aperture and $\tau_0 = 0$ at the aperture edge.

De Meulenaere and van Bladel [22] have calculated the electric polarizability for small apertures having a variety of shapes by solving the above equations using the finite difference method and have compared their numerical results with Cohn's experimental results. In their paper, de Meulenaere and van Bladel provide few details of their numerical method. In the course of this work, I used the finite difference method to solve equation (75) for τ_0 as outlined in Appendix 1. The normalized parameter τ_0 is related to the scalar potential, Θ_0, the tangential electric field and the equivalent electric dipole moment by the relationships

$$\Theta_0(\vec{r}) = -\sqrt{S} E_z^i \tau_0(\vec{r}) \tag{76}$$

$$E_t(\vec{r}) = \sqrt{S} E_z^i \nabla_t \tau_0(\vec{r}) \tag{77}$$

and

$$\vec{p}_e = 2E_z^i(S^{\frac{a}{2}})e_0(\tau_0)_{avg}\hat{z} \tag{78}$$

The results of these calculations are illustrated in Figures 4 and 5.

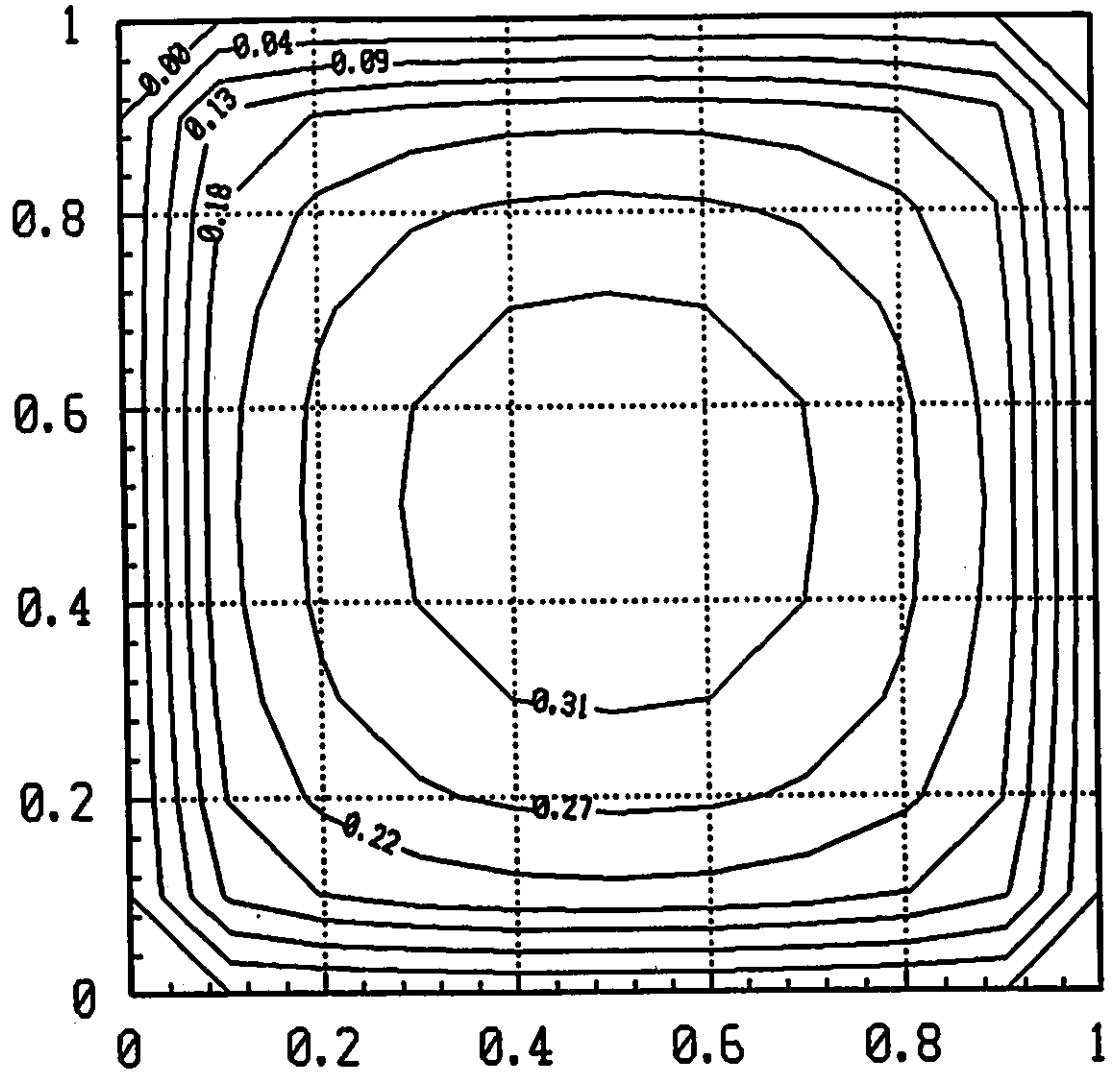

Figure 4 - Variation of τ_0 in a Square Aperture

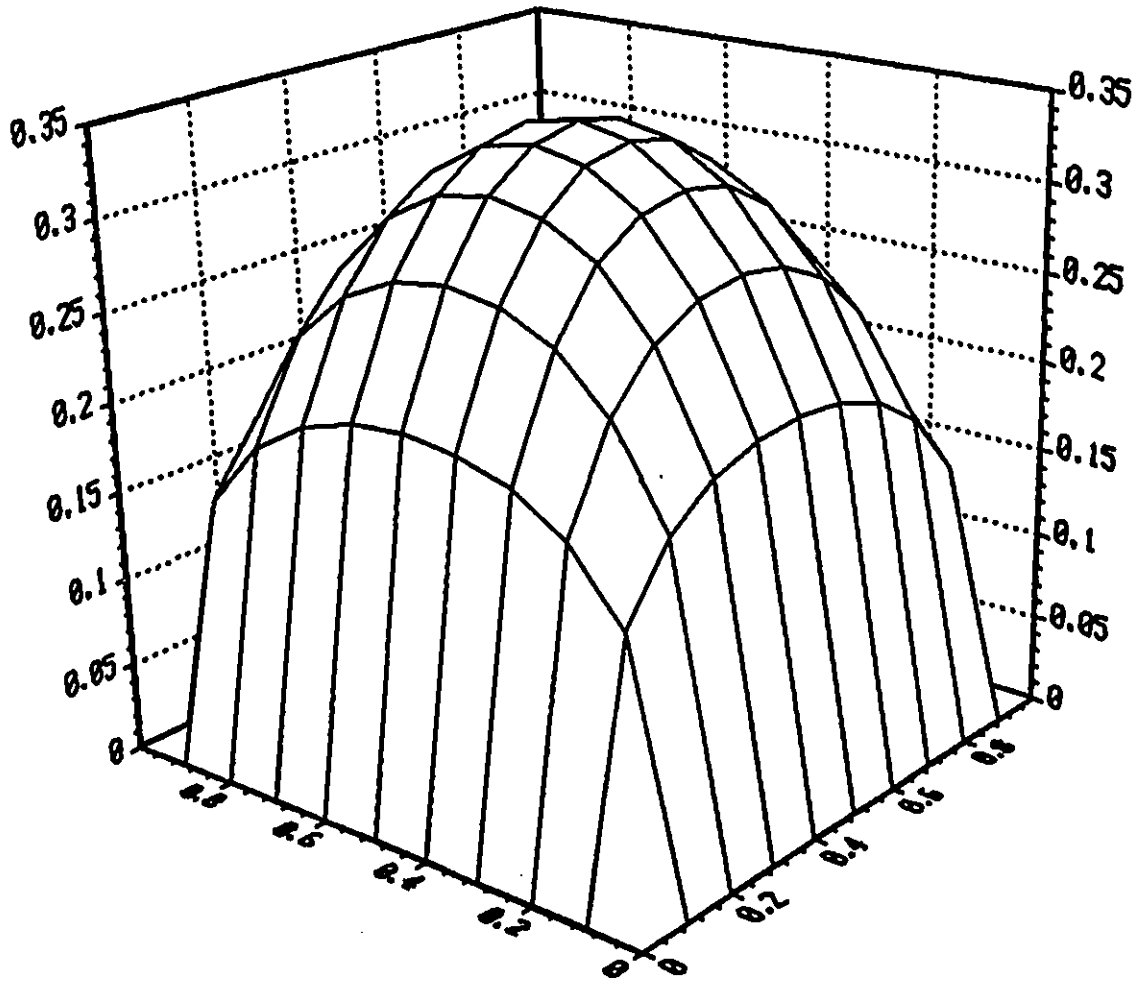

Figure 5 - Variation of τ_0 in a Square Aperture

3.2.2.2 Calculation of the Equivalent Magnetic Polarization

De Meulenaere and van Bladel also demonstrated that the following equations defined the normalised magnetic charge densities ρ_x *and* ρ_y.

$$\frac{1}{2\pi}\nabla_t\int\int_A \frac{\rho_x(\vec{r})}{|\vec{r}-\vec{r}'|}ds' = \hat{x} \tag{79}$$

and

$$\frac{1}{2\pi}\nabla_t\int\int_A \frac{\rho_y(\vec{r})}{|\vec{r}-\vec{r}'|}ds' = \hat{y} \tag{80}$$

with

$$\int\int_A \rho_x(\vec{r})ds' = \int\int_A \rho_y(\vec{r})ds' = 0 . \tag{81}$$

Once ρ_x and ρ_y are obtained, the magnetic polarizability can be obtained from the relationship

$$\vec{p} = \int\int_A \vec{r}\rho ds = \alpha_{mx}\hat{x}\hat{x} + \alpha_{my}\hat{y}\hat{y} . \tag{82}$$

Numerical results for the magnetic polarizability for a variety of aperture shapes were presented by de Meulenaere and van Bladel [22]. In this work, equations (79) and (80) were solved using the Method of Moments. Details are given in Appendix 2. The results, Figures 6 and 7, compare well with those given in [22].

Alternate methods, based on the low frequency (Rayleigh) expansion of the magnetic surface current and incident magnetic field have been proposed by Butler [23] and Rahmat-Samii and Mittra [24].

The use of the low frequency expansion method for the solution of the loaded aperture problem was investigated in this work. I concluded that this method was not suitable since higher order terms had to be retained.

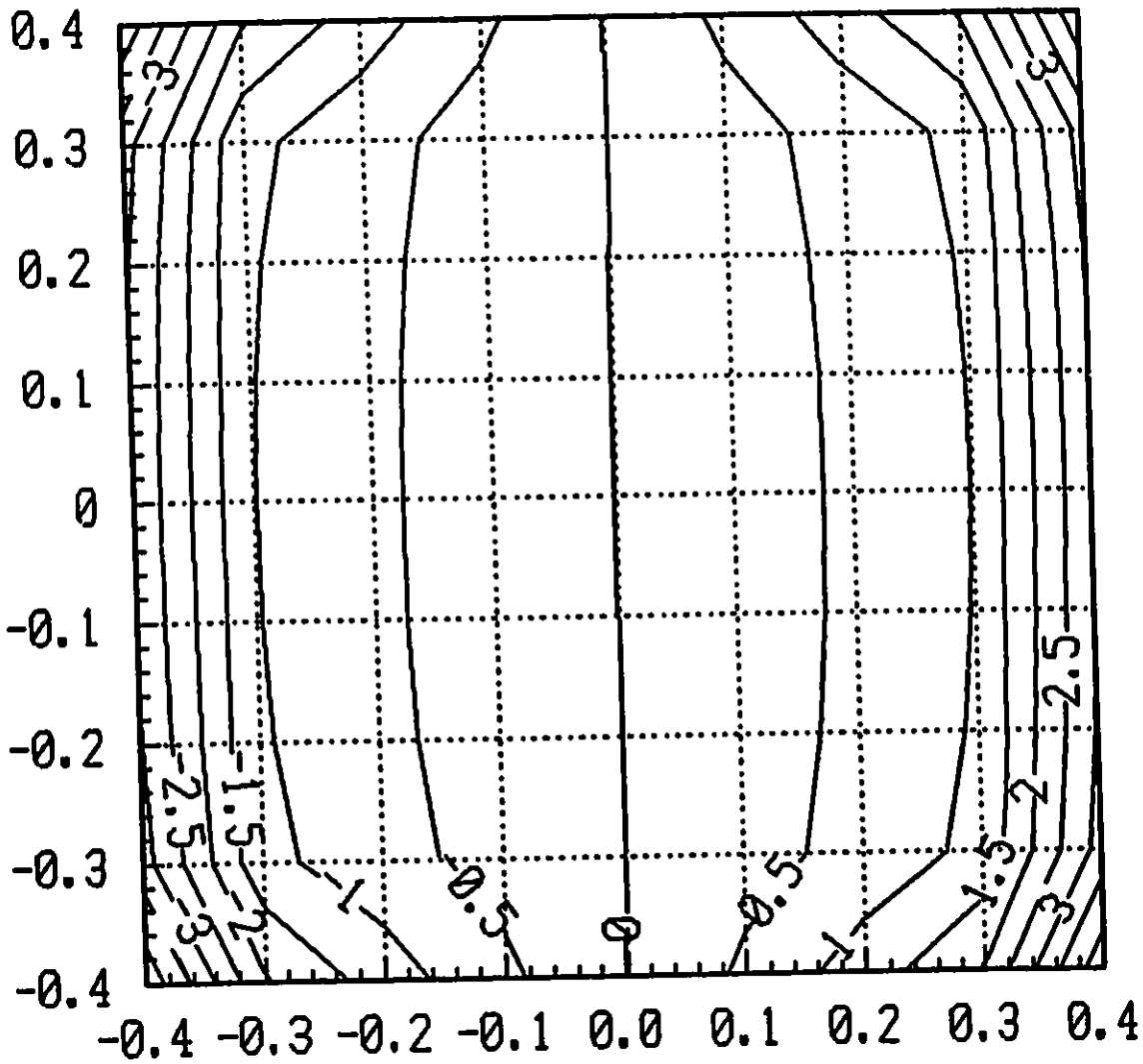

Figure 6 - Variation of $\rho_x(x,y)$ in a Square Aperture

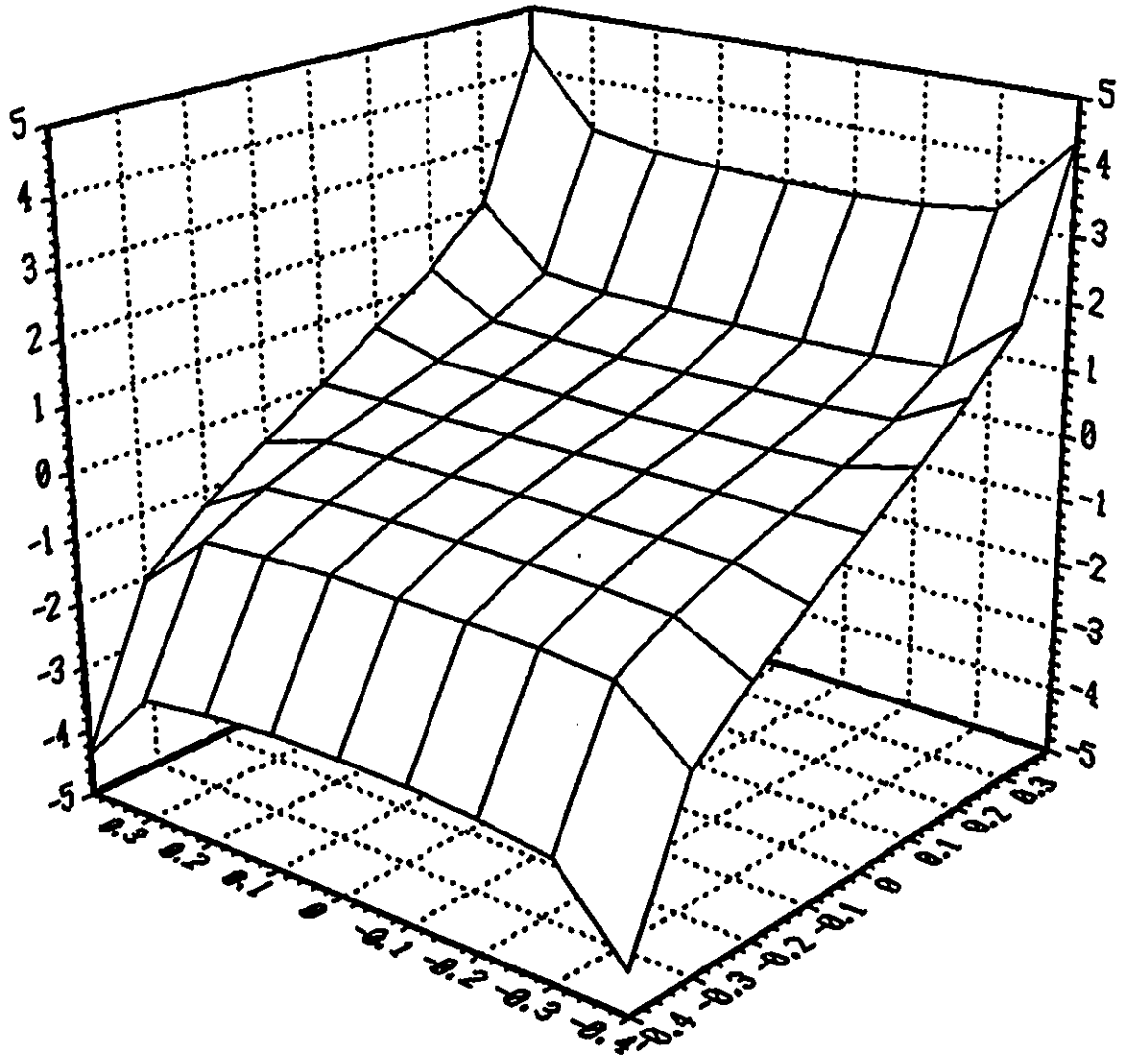

Figure 7 - Variation of $\rho_x(x,y)$ in a Square Aperture

3.2.3 Solution by the Method of Moments

The penetration of EM fields through apertures of arbitrary size has been solved by Harrington and Mautz [25-27] using the Method of Moments. If we note that

$$\frac{2\pi}{e_0}\nabla_t\cdot\vec{F} = \nabla_t\cdot\int\int_A \vec{M}_s(\vec{r}')G(\vec{r},\vec{r}')ds' = \int\int_A \vec{M}_s(\vec{r}')\cdot\nabla_t G(\vec{r},\vec{r}')ds' = -\int\int_A \vec{M}_s(\vec{r}')\cdot\nabla_s' G(\vec{r},\vec{r}')ds' \tag{83}$$

but

$$\int\int_A \vec{M}_s\cdot\nabla_t' G(\vec{r},\vec{r}')ds' = -\int\int_A \nabla_t'\cdot\vec{M}_s(\vec{r}')G(\vec{r},\vec{r}')ds' \tag{84}$$

since

$$\nabla_t'\cdot\int\int_A \vec{M}_s(\vec{r}')G(\vec{r},\vec{r}')ds' = 0. \tag{85}$$

Substitution of these relationships into (19) transforms it into the following form (as used by Mautz and Harrington [26])

$$(j\omega\vec{F}(\vec{r}) + \nabla_t\phi)\times\hat{z} = \vec{H}^i\times\hat{z} \tag{86}$$

where

$$\phi = \frac{1}{2\pi\mu_0}\int\int_A \rho_m(\vec{r}')G(\vec{r},\vec{r}')ds' \tag{87}$$

and

$$\rho_m(\vec{r}') = \frac{j}{\omega}\nabla_t'\cdot\vec{M}_s(\vec{r}')\ . \tag{88}$$

Equation (86) has been solved by Mautz and Harrington using the Method of Moments. Details of their method are given in [26].

Modification of Mautz and Harrington's method to enable the magnetic surface current, $\vec{M}_s$, and aperture polarizabilities for small apertures has been attempted in this work. At low frequencies I found that poor results were obtained because of poor matrix condition. This problem has been discussed by Mosig [28]. Wilton and Glisson [29] proposed a method to overcome this difficulty however my attempts to implement this method were unsuccessful.

3.3 EM Penetration Through Loaded Apertures

There have been very few theoretical or numerical studies of the penetration of EM fields through loaded apertures.

One of the earliest works was that of Latham and Lee [30] who studied the penetration of low frequency magnetic fields into a semi-infinite circular pipe covered with a resistive cap. To solve this problem, Latham and Lee derived an appropriate set of boundary conditions by integrating Maxwell's equations through the thickness of the cap. Using these boundary conditions, as well as Green's theorem, Latham and Lee obtained a coupled set of integro-differential equations which they then solved by the method of eigenvalue expansion. One of the major results of this work was the prediction of an inverse frequency dependence for the magnitude of the magnetic field inside the pipe when covered with a resistive sheet.

Casey [12,31] treated analytically the penetration of low frequency EM fields through a small circular aperture in an infinite screen loaded with a bonded wire mesh. He showed that the low frequency penetration of magnetic and electric fields could be reduced to the problem of solving a Fredholm integral equation. In his treatment, Casey took into account the contact resistance between the aperture rim and the material being used to load the aperture. Casey also obtained expressions for the aperture polarizabilities and magnetic and electric insertion losses from the solutions of the equations. The theory of Casey [12] has formed the basis for the interpretation of most of the experimental studies of EM penetration through loaded apertures.

Recently Gobin, Alliot and Degauque [32] have presented numerical results, based on the Method of Moments, for the penetration of EM fields through loaded apertures. In their approach, they calculated directly the equivalent magnetic current distributed on the surface of the aperture. The formulation of Gobin et. al. considered the surface impedance of the material as well as the contact resistance between the material and the aperture rim.

Chapter 4:
Numerical Solution of the Aperture Equations

4.1 Solutions for an Open Aperture

4.1.1 The Irrotational Component of $\vec{M}_s$

Noting that $\vec{F}=\hat{x}F_x+\hat{y}H_y$ and $\nabla_t=\hat{x}\frac{\partial}{\partial x}+\hat{y}\frac{\partial}{\partial y}$ then, by writing out x and y-components of (28), the following pair of equations is obtained

$$\frac{j\omega}{k^2}\left[\frac{\partial^2 F_x}{\partial x^2}+\frac{\partial^2 F_y}{\partial x \partial y}\right] = H_x^i \tag{89}$$

and

$$\frac{j\omega}{k^2}\left[\frac{\partial^2 F_y}{\partial y^2}+\frac{\partial^2 F_x}{\partial x \partial y}\right] = H_y^i \ . \tag{90}$$

If it is further assumed that the incident magnetic field can be written as

$$\vec{H}_t^i = \hat{y}e^{-jkx} = \hat{y}(1-jkx) \tag{91}$$

then the irrotational component of $\vec{H}_t^i$ becomes

$$H_{t,I}^y = 1 \ . \tag{92}$$

Expressing the electric vector potential, $\vec{F}$, in terms of the magnetic surface current using (2) allows equations (89) and (90) to be rewritten in the form

$$\frac{\partial^2}{\partial y^2}\int\int_A \frac{M_s^y}{|r-r'|}ds' + \frac{\partial^2}{\partial x \partial y}\int\int_A \frac{M_s^x}{|r-r'|}ds' = -j2\pi k\eta \tag{93}$$

and

$$\frac{\partial^2}{\partial x^2}\int\int_A \frac{M_s^x}{|r-r'|}ds' + \frac{\partial^2}{\partial x \partial y}\frac{M_s^y}{|r-r'|}ds' = 0 \ . \qquad (94)$$

In deriving (93) and (94), the approximation that $e^{-jkR} \approx 1$ has been used. This approximation is equivalent to keeping the first term in the Rayleigh expansion and is valid only for small apertures.

If the derivative terms are replaced by the finite difference approximations

$$\frac{\partial^2 f_{m,n}}{\partial x^2} = \frac{f_{m+1,n} - 2f_{m,n} + f_{m-1,n}}{h^2} \qquad (95)$$

$$\frac{\partial^2 f_{m,n}}{\partial y^2} = \frac{f_{m,n+1} - 2f_{m,n} + f_{m,n-1}}{h^2} \qquad (96)$$

and

$$\frac{\partial^2 f_{m,n}}{\partial x \partial y} = \frac{f_{m+1,n+1} - f_{m+1,n-1} - f_{m-1,n+1} + f_{m-1,n-1}}{4h^2} \ . \qquad (97)$$

then the finite difference approximation of (93) and (94) at the observation points (x_m, y_n) and (x_o, y_p) are

$$\int\int_A M_s^x K_1(x_m, y_n | x', y')\, dx'dy' + \int\int_A M_s^y K_2(x_o, y_p | x', y')\, dx'dy' = 0 \qquad (98)$$

and

$$\int\int_A M_s^x K_2(x_m, y_n | x', y')\, ds' + \int\int_A M_s^y K_3(x_o, y_p | x', y')\, ds' = -j2\pi k\eta \qquad (99)$$

where

$$\mathbf{K}_1(x_m, y_n|x', y') = \frac{h(x_{m+1}, y_n|x', y') - 2h(x_m, y_n|x', y') + h(x_{m-1}, y_n|x', y')}{h^2} \tag{100}$$

and

$$h(x_m, y_n|x', y') = \frac{1}{\sqrt{(x_m - x')^2 + (y_n - y')^2}} \ . \tag{101}$$

The definitions for the other $\mathbf{K}_n$ are similar.

I solved equations (98) and (99) using the Method of Moments by expanding $\vec{M}_s^x$ and M_s^y in terms of two dimensional pulse functions as shown below.

$$M_s^x(x, y) = \sum_i \sum_j \alpha(x_i, y_j) f(x_i, y_j) \tag{102}$$

and

$$M_s^y = \sum_k \sum_l \beta(x_k, y_l) f(x_k, y_l) \tag{103}$$

where

$$f(x_i, y_j) = P(x_i) P(y_j) \ . \tag{104}$$

where $f(x_i,y_j)$ equals 1 on S_{ij} and equals zero elsewhere.

In carrying out this calculation, I have used different grids for M_s^x and M_s^y as proposed by Wilton and Glisson [33]. This grid provides better resolution at the boundary where the fields are tangential (and hence go to infinity).

Substitution of the expressions for M_s^x and M_s^y into (98) and (99) yields the following system of equations

$$\sum_I \sum_J \alpha_{IJ} \int\int_A K_1(x_m, y_n | x', y')\, ds' + \sum_k \sum_I \int\int_A K_2(x_o, y_p | x', y')\, ds' = 0 \quad \textbf{(105)}$$

and

$$\sum_I \sum_J \alpha_{IJ} \int_{\Delta S_{IJ}} \int K_2(x_m, y_n | x', y')\, ds' + \sum_k \sum_I \beta_{kl} \int_{\Delta S_{kl}} \int K_3(x_o, y_p | x', y')\, ds' = -j2\pi k\eta \ . \quad \textbf{(106)}$$

The integrals above were evaluated using the relationship

$$\int\int \frac{dxdy}{r} = x\log(y+r) + y\log(x+r) \ . \quad \textbf{(107)}$$

Appendix 3 gives a program to solve the above set of equations for an open, square aperture. Aperture size and frequency must be specified. The frequency must be low enough so that the small aperture approximation is valid (ie. size not much larger than 0.1λ). Using this program the following points have been noted:

i) Stability at Low Frequencies: The solution for $\vec{M}_s$ is stable even at very low frequencies. This was not the case with the method used by Harrington and Mautz which was found to be unstable because of poor matrix condition. Results are shown in Tables 1 and 2 for calculation of the magnetic surface currents in a 15 cm square aperture at 2 MHz and 200 MHz.

M_s^x and M_s^y are purely imaginary as expected. The distribution of the magnetic current in the aperture is illustrated in Figures 8 and 9.

```
The recip. cond. num. was  0.28E-01

Frequency =      2.0000 MHz
Aperture Size =     15.0000 cm
Conductivity = 0.0000E+00 mho-cm

real Mx
 0.0000E+00  0.0000E+00  0.0000E+00  0.0000E+00  0.0000E+00  0.0000E+00
 0.0000E+00  0.0000E+00  0.0000E+00  0.0000E+00  0.0000E+00  0.0000E+00
 0.0000E+00  0.0000E+00  0.0000E+00  0.0000E+00  0.0000E+00  0.0000E+00
 0.0000E+00  0.0000E+00  0.0000E+00  0.0000E+00  0.0000E+00  0.0000E+00
 0.0000E+00  0.0000E+00  0.0000E+00  0.0000E+00  0.0000E+00  0.0000E+00
sumxr=  0.0000E+00

imag Mx

 0.2258E+01  0.2044E+01  0.2029E+01  0.2029E+01  0.2044E+01  0.2258E+01
 0.2847E+01  0.2811E+01  0.2832E+01  0.2832E+01  0.2811E+01  0.2847E+01
 0.3030E+01  0.3048E+01  0.3089E+01  0.3089E+01  0.3048E+01  0.3030E+01
 0.2847E+01  0.2811E+01  0.2832E+01  0.2832E+01  0.2811E+01  0.2847E+01
 0.2258E+01  0.2044E+01  0.2029E+01  0.2029E+01  0.2044E+01  0.2258E+01
sumxi=  0.7761E+02

real My
 0.0000E+00  0.0000E+00  0.0000E+00  0.0000E+00  0.0000E+00  0.0000E+00
 0.0000E+00  0.0000E+00  0.0000E+00  0.0000E+00  0.0000E+00  0.0000E+00
 0.0000E+00  0.0000E+00  0.0000E+00  0.0000E+00  0.0000E+00  0.0000E+00
 0.0000E+00  0.0000E+00  0.0000E+00  0.0000E+00  0.0000E+00  0.0000E+00
 0.0000E+00  0.0000E+00  0.0000E+00  0.0000E+00  0.0000E+00  0.0000E+00
sumyr=  0.0000E+00

imag My
 0.9644E+00  0.6280E+00  0.2174E+00 -0.2174E+00 -0.6280E+00 -0.9644E+00
 0.4014E+00  0.2963E+00  0.1053E+00 -0.1053E+00 -0.2963E+00 -0.4014E+00
-0.1810E-06 -0.1234E-05 -0.5377E-06 -0.4037E-06  0.1166E-06 -0.4394E-06
-0.4014E+00 -0.2963E+00 -0.1053E+00  0.1053E+00  0.2963E+00  0.4014E+00
-0.9644E+00 -0.6280E+00 -0.2174E+00  0.2174E+00  0.6280E+00  0.9644E+00
sumyi= -0.5186E-05
```

Table 1 - Magnetic Surface Currents for an Square Open Aperture (2 MHz)

```
The recip. cond. num. was  0.28E-01

Frequency =    200.0000 MHz
Aperture Size =     15.0000 cm
Conductivity = 0.0000E+00 mho-cm

real Mx
 0.0000E+00  0.0000E+00  0.0000E+00  0.0000E+00  0.0000E+00  0.0000E+00
 0.0000E+00  0.0000E+00  0.0000E+00  0.0000E+00  0.0000E+00  0.0000E+00
 0.0000E+00  0.0000E+00  0.0000E+00  0.0000E+00  0.0000E+00  0.0000E+00
 0.0000E+00  0.0000E+00  0.0000E+00  0.0000E+00  0.0000E+00  0.0000E+00
 0.0000E+00  0.0000E+00  0.0000E+00  0.0000E+00  0.0000E+00  0.0000E+00
sumxr=  0.0000E+00

imag Mx

 0.2258E+03  0.2044E+03  0.2029E+03  0.2029E+03  0.2044E+03  0.2258E+03
 0.2847E+03  0.2811E+03  0.2832E+03  0.2832E+03  0.2811E+03  0.2847E+03
 0.3030E+03  0.3048E+03  0.3089E+03  0.3089E+03  0.3048E+03  0.3030E+03
 0.2847E+03  0.2811E+03  0.2832E+03  0.2832E+03  0.2811E+03  0.2847E+03
 0.2258E+03  0.2044E+03  0.2029E+03  0.2029E+03  0.2044E+03  0.2258E+03
sumxi=  0.7761E+04

real My
 0.0000E+00  0.0000E+00  0.0000E+00  0.0000E+00  0.0000E+00  0.0000E+00
 0.0000E+00  0.0000E+00  0.0000E+00  0.0000E+00  0.0000E+00  0.0000E+00
 0.0000E+00  0.0000E+00  0.0000E+00  0.0000E+00  0.0000E+00  0.0000E+00
 0.0000E+00  0.0000E+00  0.0000E+00  0.0000E+00  0.0000E+00  0.0000E+00
 0.0000E+00  0.0000E+00  0.0000E+00  0.0000E+00  0.0000E+00  0.0000E+00
sumyr=  0.0000E+00

imag My
 0.9644E+02  0.6280E+02  0.2174E+02 -0.2174E+02 -0.6280E+02 -0.9644E+02
 0.4014E+02  0.2963E+02  0.1053E+02 -0.1053E+02 -0.2963E+02 -0.4014E+02
-0.6154E-05 -0.1153E-03 -0.5773E-04 -0.3802E-04  0.2141E-04 -0.3359E-04
-0.4014E+02 -0.2963E+02 -0.1053E+02  0.1053E+02  0.2963E+02  0.4014E+02
-0.9644E+02 -0.6280E+02 -0.2174E+02  0.2174E+02  0.6280E+02  0.9644E+02
sumyi= -0.3967E-03
```

Table 2 - Magnetic Surface Currents for a Square Open Aperture (200 MHz)

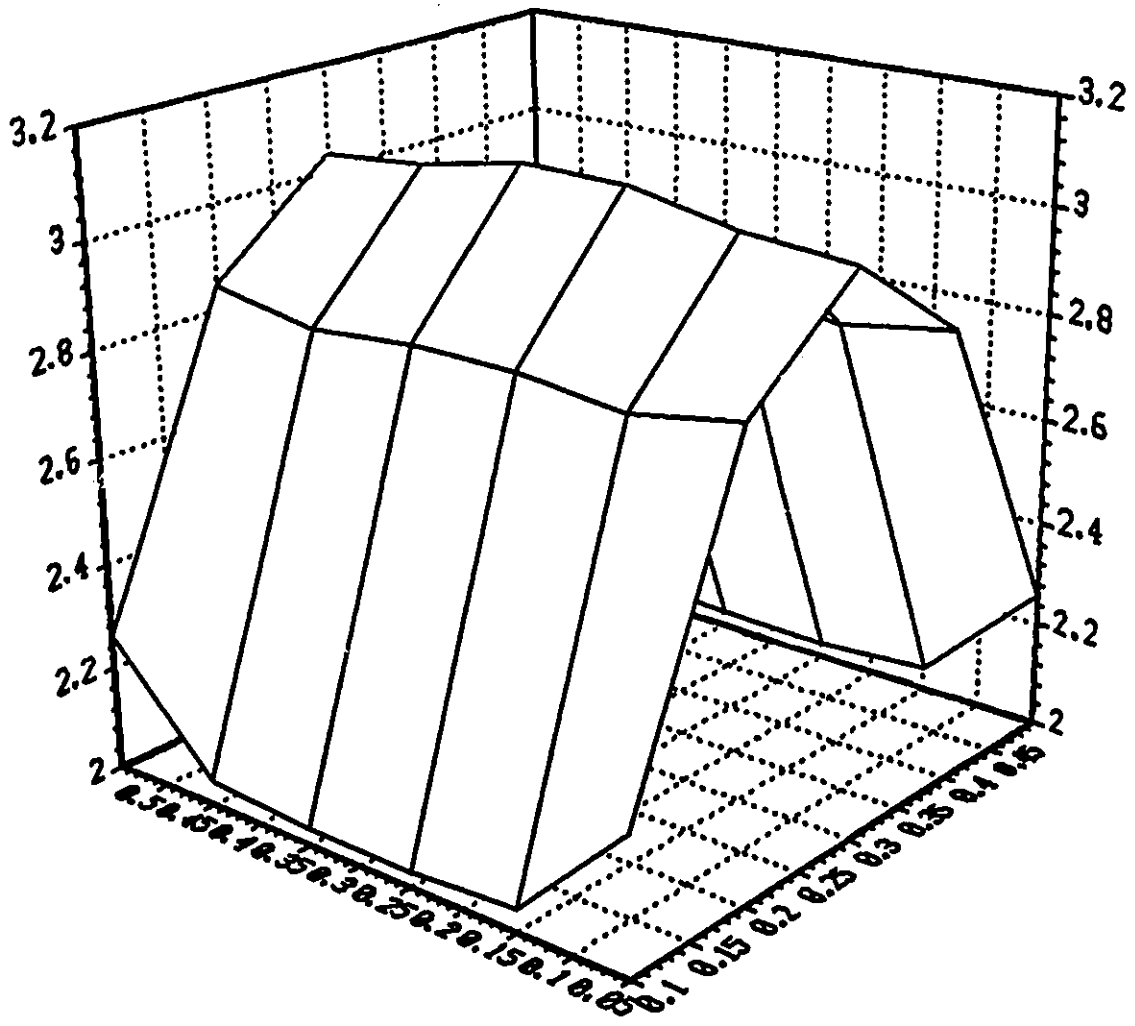

Figure 8 - X-Component of the Magnetic Surface Current in a Square Open Aperture

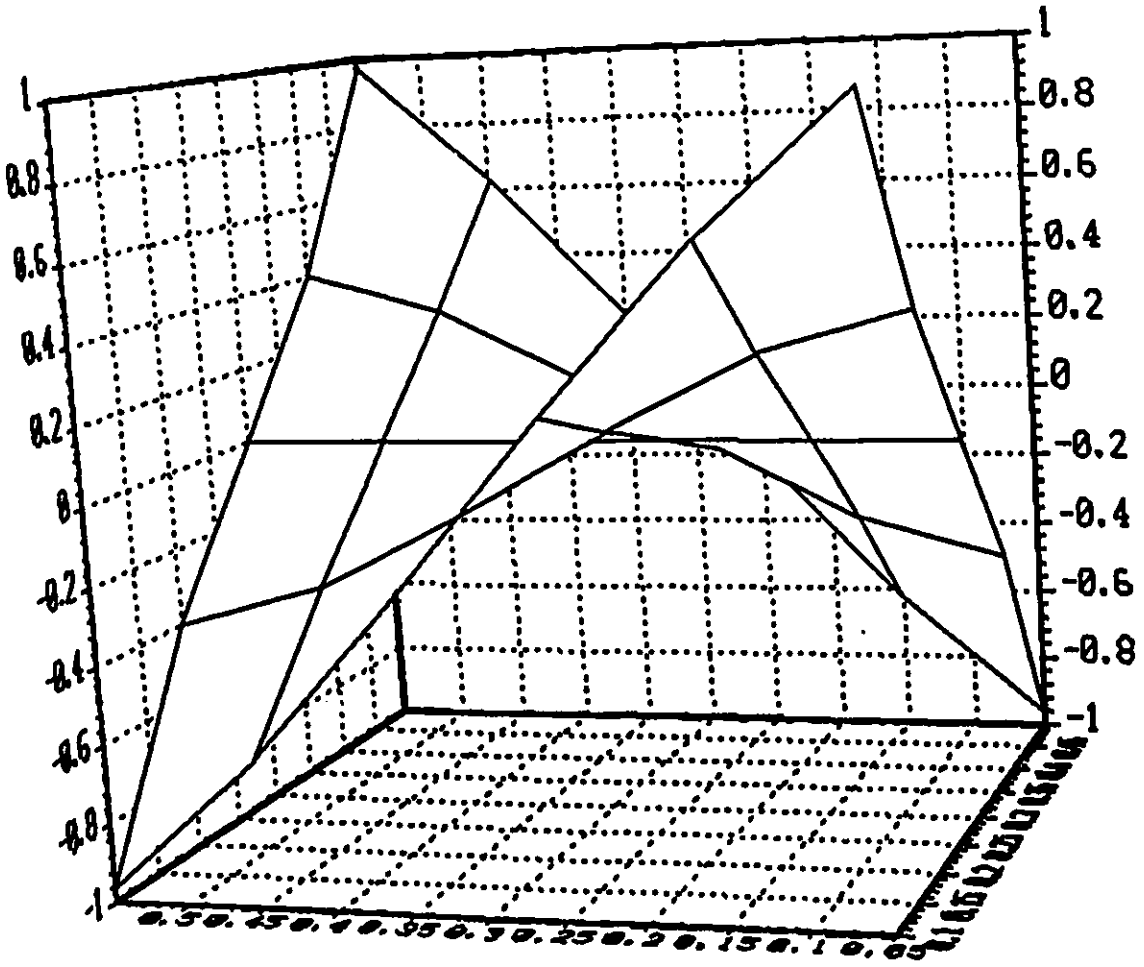

Figure 9 - Y-Component of the Magnetic Surface Current in a Square Open Aperture

ii) Effect of k^2 Term: In carrying out the above calculation, I neglected the term in k^2. To assess the validity of this approximation, I wrote a modified version of the program that included the k^2 term. Results for both programs are shown in Table 3. The results demonstrate that the neglect of the k^2 term has no penalty.

```
The recip. cond. num. was  0.28E-01

Frequency =     20.0000 MHz
Aperture Size =    15.0000 cm
Conductivity = 0.0000E+00 mho-cm
```

a) Neglecting k^2 Term

```
imag Mx

 0.2259E+02  0.2046E+02  0.2032E+02  0.2032E+02  0.2046E+02  0.2259E+02
 0.2848E+02  0.2814E+02  0.2835E+02  0.2835E+02  0.2814E+02  0.2848E+02
 0.3032E+02  0.3051E+02  0.3093E+02  0.3093E+02  0.3051E+02  0.3032E+02
 0.2848E+02  0.2814E+02  0.2835E+02  0.2835E+02  0.2814E+02  0.2848E+02
 0.2259E+02  0.2046E+02  0.2032E+02  0.2032E+02  0.2046E+02  0.2259E+02
sumxi=  0.7769E+03
```

b) Including k^2 Term

```
imag Mx

 0.2258E+02  0.2044E+02  0.2029E+02  0.2029E+02  0.2044E+02  0.2258E+02
 0.2847E+02  0.2811E+02  0.2832E+02  0.2832E+02  0.2811E+02  0.2847E+02
 0.3030E+02  0.3048E+02  0.3089E+02  0.3089E+02  0.3048E+02  0.3030E+02
 0.2847E+02  0.2811E+02  0.2832E+02  0.2832E+02  0.2811E+02  0.2847E+02
 0.2258E+02  0.2044E+02  0.2029E+02  0.2029E+02  0.2044E+02  0.2258E+02
sumxi=  0.7761E+03
```

Table 3 - Effect of k^2 Term on Calculation of Magnetic Surface Current

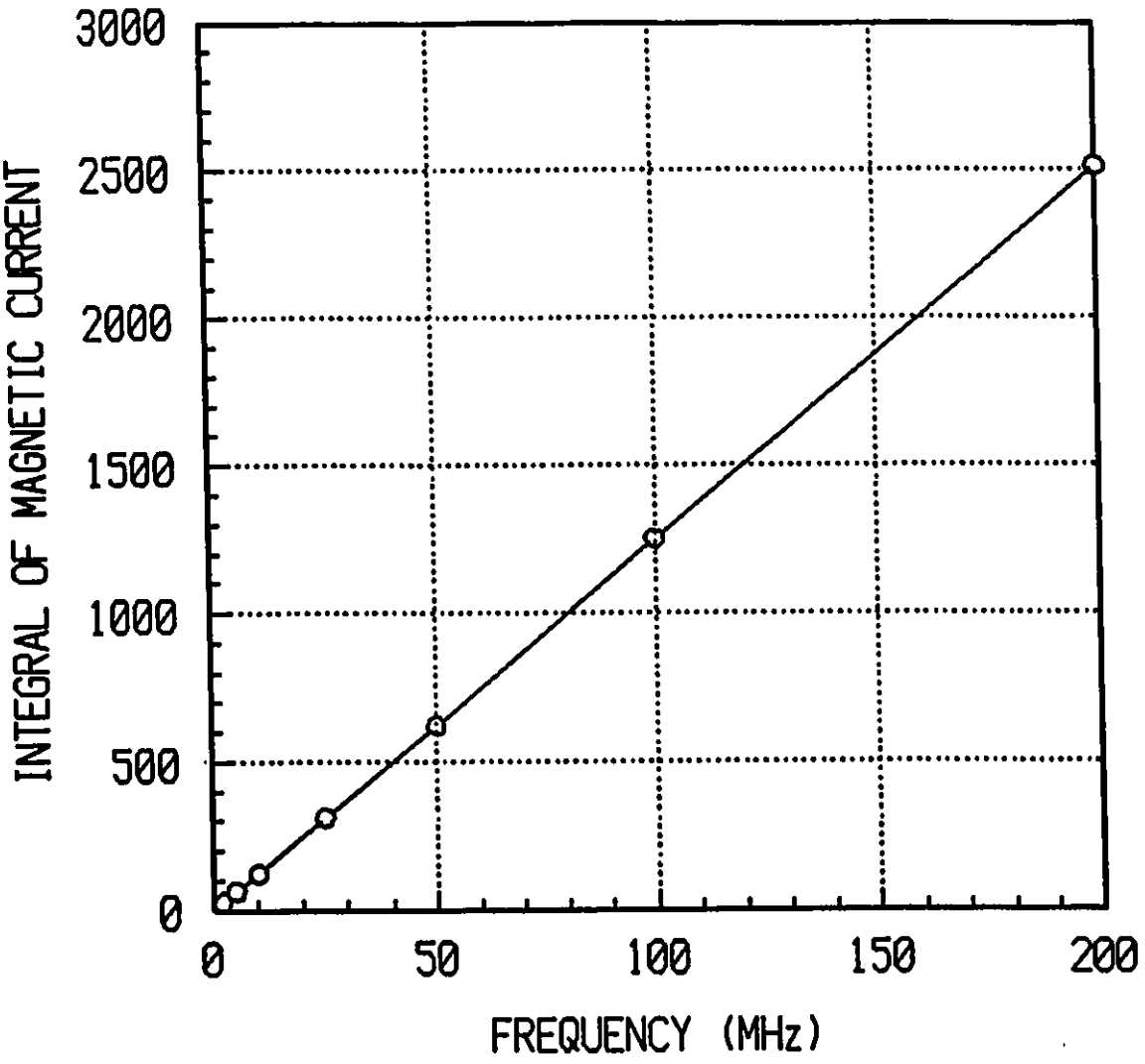

Figure 10 - Frequency Dependence of the Integral of the Magnetic Surface Current

iii) Equivalent Dipole Moments and Polarizabilities: The magnetic dipole moment is related to the irrotational component of the magnetic surface current by the relationship shown below

$$\vec{p}_m = -\frac{1}{\omega\mu}\iint_A \vec{M}_{s,I}(r')\,ds' \qquad (108)$$

Since the equivalent magnetic dipole moment, $\vec{p}_m$, is independent of frequency (ie. only dependent on aperture size), the integral of $\vec{M}_s$ should be linearly dependent on frequency. The calculated results shown in Figure 10 are in agreement with this prediction. The magnetic polarizability for a 15 cm square aperture is calculated to be 614 cm^3. This can be compared to the analytical results for an equivalent area circular aperture which has an equivalent magnetic polarizability of 404 cm^3. The results are in reasonable agreement.

4.1.2 The Solenoidal Component of $\vec{M}_s$

To obtain the solenoidal component of $\vec{M}_s$, the following equation must be solved

$$\iint_A \frac{M_s^y}{|r-r'|} dx'dy' = -2\pi\eta x \ . \tag{109}$$

This equation can be solved using the Method of Moments as before. The magnetic surface current, M_s^y, is expanded using two dimensional pulse functions as before

$$M_s^y(x,y) = \sum_{n=1}^{N} \alpha_n f_n(x,y) \tag{110}$$

where $f_n(x,y)$ equals 1 on s_n and equals zero elsewhere.

Substituting this expression for M_s^y into (109) yields the following

$$\sum_{n=1}^{N} \alpha_n \iint_A f_n(x',y')\, k(x,y|x',y')\, ds' - \sum_{n=1}^{N} \alpha_n \int_{\Delta s_n} \int h(x,y|x',y')\, ds' = -2\pi\eta x \tag{111}$$

Using δ-functions for testing or applying colocation leads to the following set of linear equations that must be solved

$$\sum_{n=1}^{N} \alpha_n \int_{\Delta S_n} \int h(x_m, y_m | x', y')\, ds' = -2\pi\eta x \qquad (112)$$

where

$$h(x_m, y_m | x', y') = \frac{1}{\sqrt{(x_m - x')^2 + (y_m - y')^2}} \,. \qquad (113)$$

Equation (112) can be rewritten in the form

$$\sum_{n=1}^{N} \alpha_n K_{mn} = -2\pi\eta x_m \qquad (114)$$

where

$$K_{mn} = \int_{\Delta S_n} \int h(x_m, y_m | x', y')\, dx' dy' \,. \qquad (115)$$

This system of equations can be solved once the coefficients, K_{mn}, can be evaluated. To do this the following approximations have been made.

i) For m $\neq$ n

$$K_{mn} = \int_{\Delta S_n} \int \frac{1}{\sqrt{(x_m - x')^2 + (y_m - y')^2}} dx' dy' = \frac{\Delta S_n}{\sqrt{(x_m - x_n)^2 + (y_m - y_n)^2}} \qquad (116)$$

ii) For m = n

When m = n, the above approximation is not valid as a singularity occurs when the source and observation points coincide. To approximate this integral, consider a circular region of radius, a, surrounding the observation point. Then

$$K_{mn} = \int_0^a \int_0^{2\pi} \frac{1}{R} R dR d\Theta = 2\pi a \ . \qquad (117)$$

Equating equivalent areas for the square and circular regions gives

$$a = \frac{1}{\sqrt{\pi}} \qquad and \qquad K_{mn} = 2\sqrt{\pi} \ . \qquad (118)$$

Appendix 4 gives a program to determine the solenoidal component of $\vec{M}_s$ in an square open aperture using the approximations given above. Aperture size and frequency must be specified and the aperture must be electrically small. The following points are noted from these calculations.

i) Stability at Low Frequency: The solution for the solenoidal component of $\vec{M}_s$ is stable at low frequency. The distribution of the solenoidal component in the aperture is shown in Figure 11.

ii) Equivalent Dipole Moment and Polarizability: Using the data for the solenoidal component of $\vec{M}_s$, the equivalent electric dipole moment, p_e, can be obtained from equation (8). Using the data, an equivalent electric polarizability was found to be 167 cm^3 for a 15 cm square aperture. This is in reasonable agreement with the analytical value of 202 cm^3 for an equal area circular aperture.

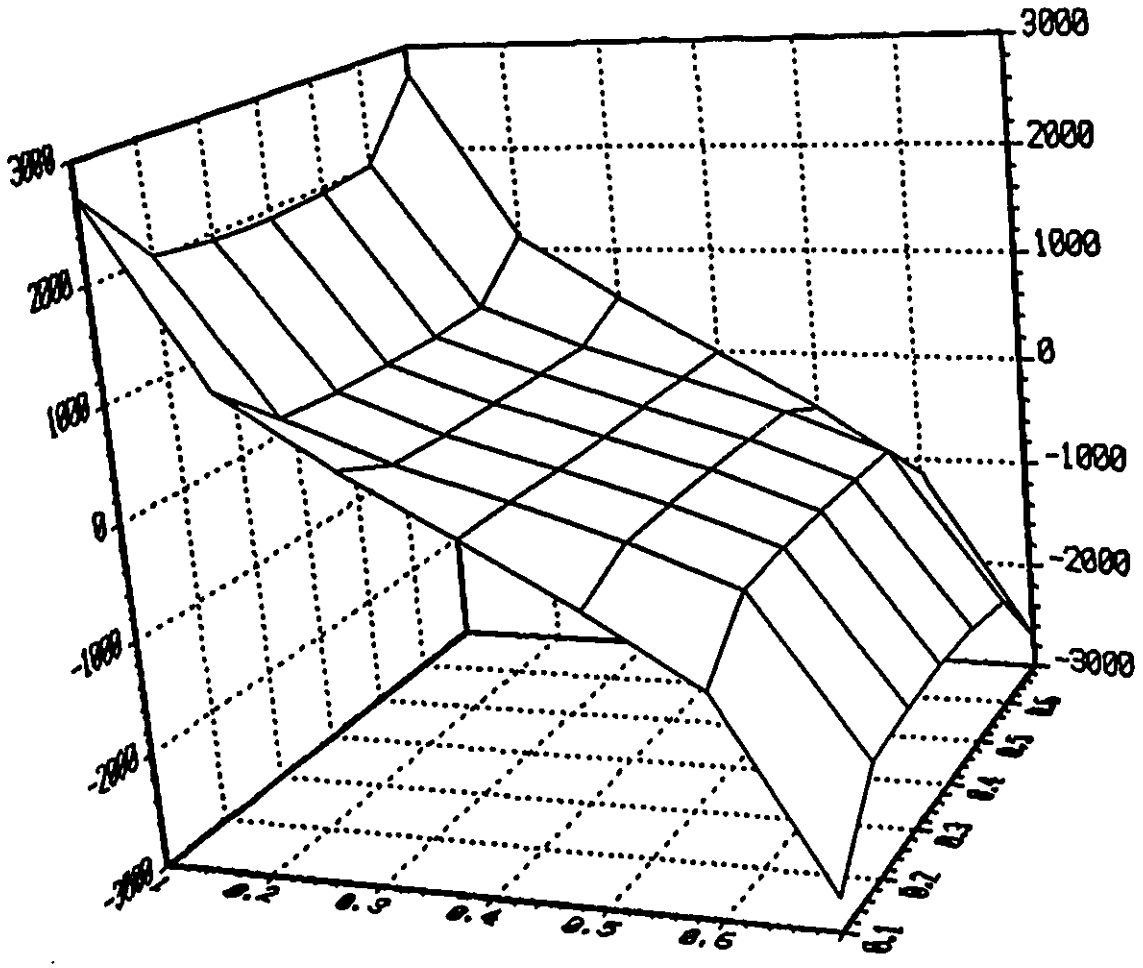

Figure 11 - The Solenoidal Component of the $\vec{M}_s$ in an Square, Open Aperture

4.2 Solutions for a Loaded Aperture:

4.2.1 Calculation of the Irrotational Component of $\vec{M}_s$:

4.2.1.1 An Isotropic Resistive Sheet

Using the methods used in section 4.1, (44) reduces to the following system of equations

$$\frac{\partial^2}{\partial y^2}\int\int_A \frac{M_s^y}{|r-r'|}ds' + \frac{\partial^2}{\partial y^2}\int\int_A \frac{M_s^x}{|r-r'|}ds' + j\pi k\eta\sigma_s M_s^y = -j2\pi k\eta \qquad (119)$$

$$\frac{\partial^2}{\partial x^2}\int\int_A \frac{M_s^x}{|r-r'|}ds' + \frac{\partial^2}{\partial x\partial y}\int\int_A \frac{M_s^y}{|r-r'|}ds' + j\pi k\eta\sigma_s M_s^y = 0 \ . \qquad (120)$$

Expanding $\vec{M}_s$ in terms of pulse functions and using δ-functions for testing leads to the following set of linear equations to be solved

$$\sum_{i,j}\alpha_{ij}\int_{\Delta S_{ij}}\int K_1 ds' + \sum_{k,l}\beta_{kl}\int_{\Delta S_{kl}}\int K_2 ds' + j\pi k\eta\sigma_s\alpha_{mn} = 0 \qquad (121)$$

$$\sum_{i,j}\alpha_{ij}\int_{\Delta S_{ij}}\int K_2 ds' + \sum_{k,l}\beta_{kl}\int_{\Delta S_{kl}}\int K_3 ds' + j\pi k\eta\sigma_s\beta_{kl} = -j2\pi k\eta \ . \qquad (122)$$

The following points are noted.

i) When pulse functions are used for expansion and δ-functions for testing, aperture loading only modifies the diagonal elements of the Moment Method (S) matrix as shown below.

$$S\phi = b \qquad (123)$$

where

$$S_{mn}^{\alpha} = \int_{\Delta S_{mn}} \int K_1 ds' + j\pi k\eta\sigma_s \tag{124}$$

and

$$S_{mn}^{\beta} = \int_{\Delta S_{mn}} \int K_3 ds' + j\pi k\eta\sigma_s \ . \tag{125}$$

The above equations show that, if the diagonal elements are dominant, then the ratio of the magnetic currents in the open and loaded apertures is

$$\frac{M_{mn}^{y}}{\tilde{M}_{mn}^{y}} = \left[1 + \frac{j\pi k\eta\sigma_s}{\iint K_1 ds'}\right] \ . \tag{126}$$

Compare this expression with the expression given by Casey [12] for the ratio of the equivalent magnetic polarizability for open, circular aperture and for a circular aperture loaded with a resistive sheet

$$\frac{\alpha_m}{\tilde{\alpha}_m} = \left[1 + \frac{j4\pi\omega\mu_0 r\sigma}{3\pi}\right] \ . \tag{127}$$

The similarity in form of (126) and (127) is obvious.

As part of this work, I have written computer programs to calculate the irrotational component of the magnetic surface current as well as the magnetic insertion loss of a resistive sheet defined by

$$IL_m = 20\log\frac{\alpha_m}{\tilde{\alpha}_m} \ . \tag{128}$$

Results for the magnetic insertion loss of an isotropic resistive sheet are shown in Figure 12 for several different values of surface conductivity. The most notable feature of these curves is the linear dependence of the magnetic insertion loss on frequency for materials with high conductivity. These results are in agreement with experimental results presented later.

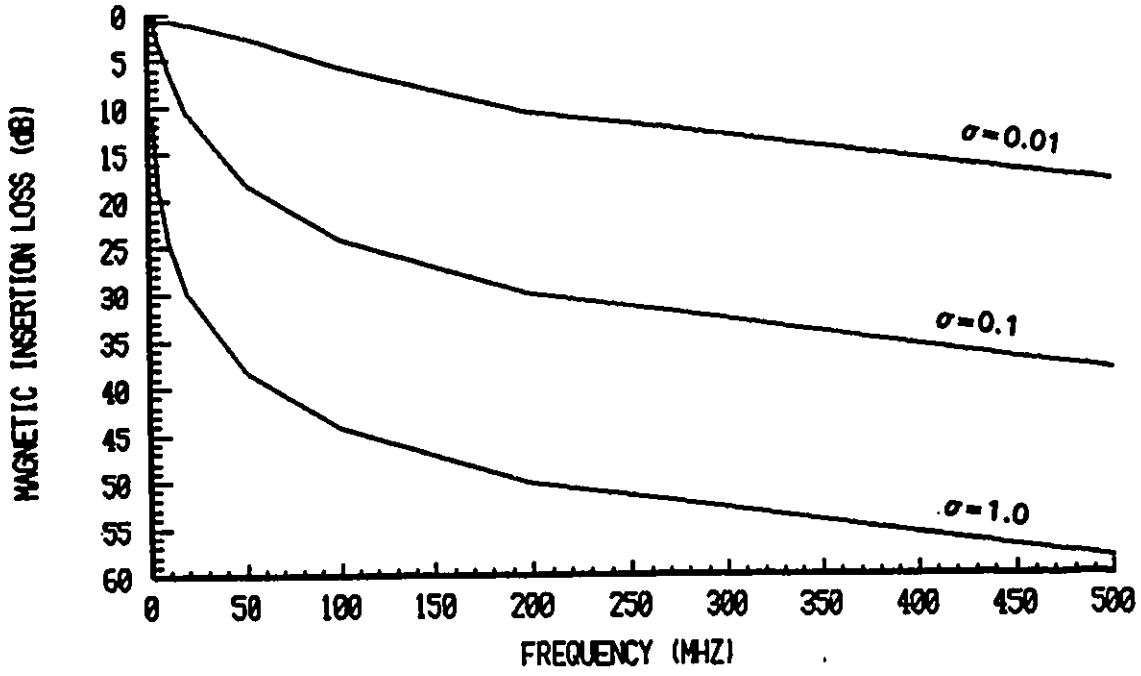

Figure 12 - Magnetic Insertion Loss of an Isotropic Resistive Material as a Function of Resistivity

4.2.1.2 An Anisotropic Resistive Sheet

The basic equations for the calculation of the magnetic surface current when the aperture is loaded with an anisotropic, resistive sheet have been given in section 2.5.2.2. If the direction of propagation of the EM wave is at an angle θ to the fibre (x) direction, the (unit) magnetic field, $\vec{H}^{i}_{t,I}$, can be written

$$\vec{H}^{i}_{t,I} = \hat{x}\sin\theta + \hat{y}\cos\theta \ . \qquad (128)$$

Following the method used in the previous section, the vector equation (49) reduces to the following pair of (scalar) equations:

$$\frac{\partial^2}{\partial y^2}\iint_A \frac{M^y_s}{|r-r'|}ds' + \frac{\partial^2}{\partial y^2}\iint_A \frac{M^x_s}{|r-r'|}ds' + j\pi k\eta\sigma M^y_s = -j2\pi k\eta\cos\theta \qquad (130)$$

and

$$\frac{\partial^2}{\partial x^2}\iint_A \frac{M^x_s}{|r-r'|}ds' + \frac{\partial^2}{\partial x\partial y}\iint_A \frac{M^y_s}{|r-r'|}ds' = -j2\pi k\eta\sin\theta \ . \qquad (131)$$

These equations were solved using the Method of Moments following the procedures given in section 4.2.1.1. Numerical results for the magnetic insertion loss of an anisotropic (unidirectional) resistive material as a function of orientation are shown in Figure 13.

These results show that the shielding properties of the material degrades very rapidly when the propagation direction is not along the x-axis. The results are qualitatively correct since only the component of magnetic field that is orthogonal to the fibre direction is shielded. The component of the magnetic field parallel to the fibre passes through the material unattenuated. These numerical results are in good agreement with the experimental results that are presented in Chapter 5.

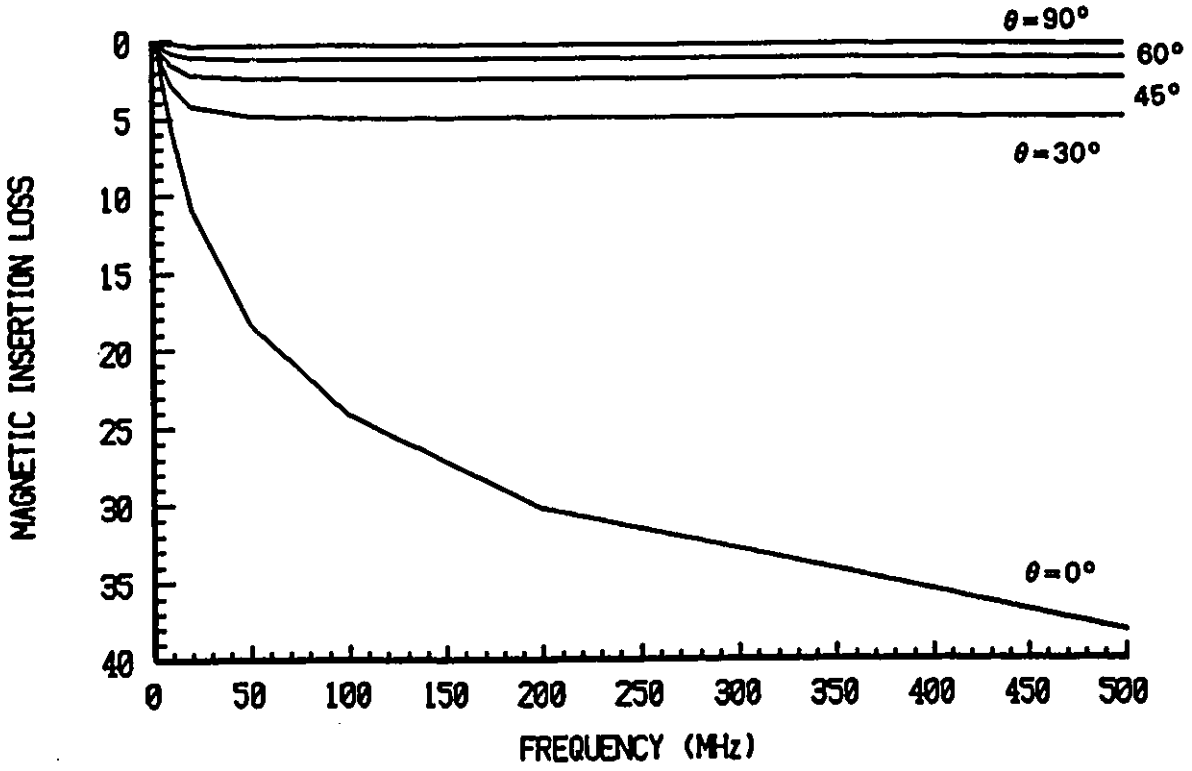

Figure 13 - Magnetic Insertion Loss of an Anisotropic Resistive Material as a Function of Orientation

4.2.1.3 Bonded and Unbonded Wire Meshes

If it is assumed that the mesh wires lie along the principal (x and y) axes of the TEM cell, then the basic equation for the calculation of the magnetic surface current, when the aperture is loaded with a bonded or an unbonded wire mesh, is given in section 2.5.2.3. Following the methods used previously, equation (63) reduces to the following pair of equations

$$\frac{\partial^2}{\partial y^2}\iint_A \frac{M_s^y}{|r-r'|}ds' + \frac{\partial^2}{\partial y^2}\iint_A \frac{M_s^x}{|r-r'|}ds' + \frac{\pi\mu_0}{L_s}M_s^y = -j2\pi k\eta \qquad (132)$$

and

$$\frac{\partial^2}{\partial x^2}\int\int_A \frac{M_s^x}{|r-r'|}ds' + \frac{\partial^2}{\partial x \partial y}\int\int_A \frac{M_s^y}{|r-r'|}ds' + \frac{\pi\mu_0}{L_s}M_s^y = 0 \ . \qquad (133)$$

As before, I solved these equations using the Method of Moments. Calculations of magnetic insertion loss were made for grid spacings that corresponded to subdivision of a 14.5 cm square aperture into 4, 16, 64, 256 and 1024 equally sized square segments. Equation (53) was used to calculate the mesh inductance using a wire radius, r_w, of 0.202 mm which corresponds to the radius of the #26 AWG wire that was used in the experimental portion of this work. Table 4 gives numerical results for the magnetic insertion loss of bonded and unbonded wire meshes. The calculated magnetic insertion loss for all of the wire meshes was found to be essentially independent of frequency over the frequency range of 2 - 500 MHz.

Table 4 - Calculated Magnetic Insertion Loss of Bonded and Unbonded Wire Meshes

Number of Wires	Insertion Loss (dB) Bonded Wire Mesh	Insertion Loss (dB) Unbonded Wire Mesh	Insertion Loss(dB) Casey's Theory (Reference 5)
1	5.74	5.74	4.95
3	9.92	9.92	9.09
7	15.85	15.85	14.99
15	23.29	23.29	22.43
31	32.06	32.06	31.20

Included in Table 4 for comparison are numerical results obtained using the theory given by Casey [12] for a small circular aperture loaded with a bonded wire mesh. In making this comparison, I have chosen the aperture radius so that the area of the circular aperture is the same as the square aperture examined here. Agreement between the numerical results calculated in this work and Casey's theory is good.

4.2.1.4 A Unidirectional Wire Grid

In this section it is assumed that a unidirectional wire grid is formed by covering the aperture with a number of equally spaced, parallel wires. From (66), the following pair of scalar equations is obtained.

$$\frac{\partial^2}{\partial y^2}\iint_A \frac{M_s^y}{|r-r'|}ds' + \frac{\partial^2}{\partial y^2}\iint_A \frac{M_s^x}{|r-r'|}ds' + \frac{\pi\mu_0}{L_s}M_s^y = -j2\pi k\eta\cos\theta \qquad (134)$$

and

$$\frac{\partial^2}{\partial x^2}\iint_A \frac{M_s^x}{|r-r'|}ds' + \frac{\partial^2}{\partial x\partial y}\iint_A \frac{M_s^y}{|r-r'|}ds' = -j2\pi k\eta\sin\theta \ . \qquad (135)$$

In the above equations, θ is the angle between the direction of propagation of the EM wave and the wire direction. In this work, magnetic insertion loss has been calculated for $\theta=0°$ and 90°. Results for the subdivision of a 14.5 cm square aperture in 2, 4, 8, 16 and 32 equally sized segments are shown in Table 5.

Table 5 - Calculated Magnetic Insertion Loss for Various Wire Grids

Number of Wires	Insertion Loss (dB) $\theta=0°$	Insertion Loss (dB) $\theta=90°$
1	5.74	0
3	9.92	0
7	15.85	0
15	23.29	0
31	32.06	0

The above results show that the insertion loss of the wire grid is the same as an equivalently spaced mesh when the wires are oriented along the direction of propagation but provides no magnetic shielding when the wires are orthogonal to the direction of propagation. This behaviour can be understood since the magnetic shielding results from the flow of current down the body of the cell as seen from (38). When the wires are orthogonal there can be no quasi-static flow of current.

4.2.2 Calculation of the Solenoidal Component of $\vec{M}_s$

4.2.2.1 Isotropic and Anisotropic Resistive Sheets

Chapter 2 has shown that the electric shielding provided by an anisotropic resistive material is independent of orientation and that the solenoidal component of the magnetic surface current for both an isotropic and an anisotropic resistive sheet is defined by equation (45).

To obtain the solenoidal component of $\vec{M}_s$ in the case of the loaded aperture, the following equation must be solved

$$\iint_A \frac{M_s^y}{|r-r'|} - \frac{j\pi\eta\sigma M_s^y}{k} = -2\pi\eta x \ . \qquad (136)$$

Solution of the above equation can be obtained using the Method of Moments as before. In this case, the loading only alters the diagonal elements of the Moment Method (S) matrix as before and that the ratio of the solenoidal components of the magnetic currents is given by

$$\frac{M_s^y}{\tilde{M}_s^y} = [1 - \frac{j\pi\eta\sigma}{k\iint K ds'}] \ . \qquad (137)$$

This shows that the solenoidal component of $\vec{M}_s$ of a resistively loaded aperture is inversely proportional to frequency and that the electric insertion loss, IL_e, defined by

$$IL_e = 20\log\frac{\alpha_e}{\tilde{\alpha}_e} \qquad (138)$$

is inversely proportional to the logarithm of the frequency when the conductivity is high.

I have written computer programs to calculate the solenoidal component of $\vec{M}_s$ and also the electric insertion loss. Figure 14 shows the electric insertion loss calculated for various sheet conductivity. The results are in general agreement with experimental measurement although the measurement of the electric shielding effectiveness is difficult, as I will discuss in the experimental section of the report.

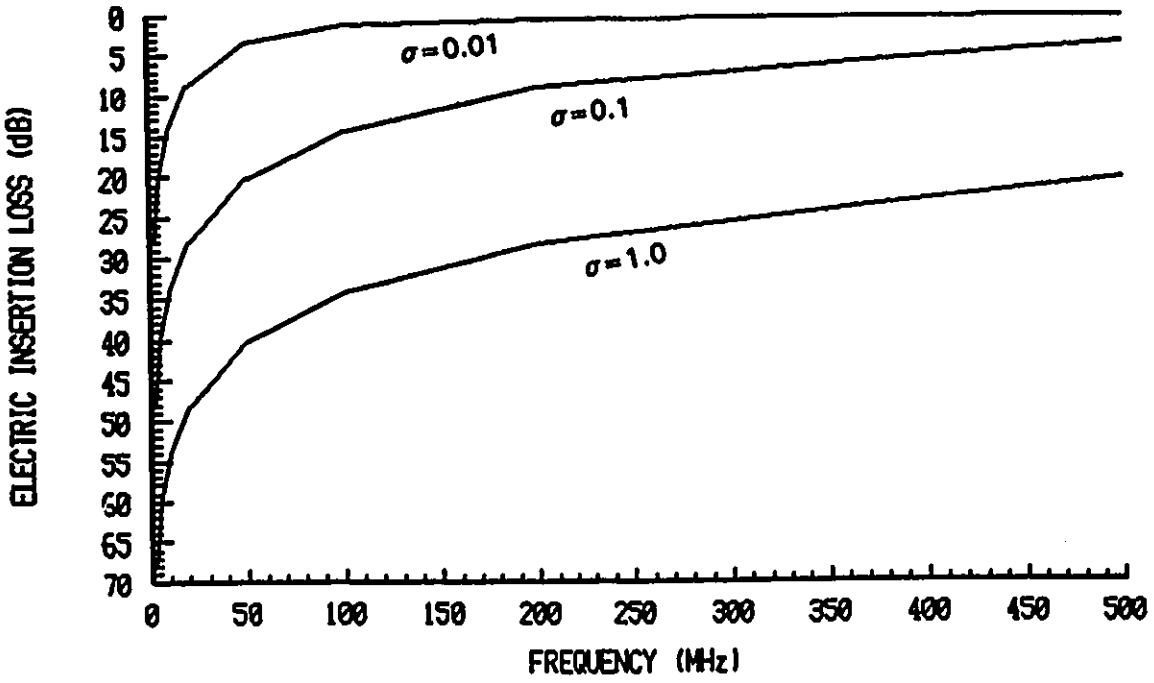

Figure 14 - Electric Insertion Loss of Resistive Sheets as a Function of Conductivity

4.2.2.2 Wire Grids and Meshes

As indicated in section 2.5.2.3, I was unable to derive a simple integral equation for the solenoidal component of $\vec{M}_s$ when the aperture was loaded with a wire grid or mesh. Numerical solution of the appropriate equations has been accomplished however using the procedure outlined below. In this discussion, the case of a bonded wire mesh is considered. Solution for an unbonded mesh or a unidirectional grid follows in a similar manner.

By taking the cross product of equation (38) with $\hat{z}$ the following equation is obtained

$$[\vec{H}_t^+(\vec{r}) - \vec{H}_s^-(\vec{r})] - \hat{z} \times \vec{J}_s - \vec{P}_s . \tag{139}$$

Substitution of (1) and (5) into (139) then yields

$$\frac{j\omega}{k^2}[\nabla_t \nabla_t \cdot \vec{F} + k^2 \vec{F}] + \frac{1}{2}\vec{P}_s - \vec{H}_t^i . \tag{140}$$

If the curl of both sides of (140) is taken (noting that $\vec{H}_t^i$ is given by (23)), then

$$j\omega \nabla_t \times \vec{F} + \frac{1}{2}\nabla_t \times \vec{P}_s - -jkH_0 . \tag{141}$$

This equation can then be integrated as before (section 2.4.2) to yield

$$j\omega F^y + \frac{1}{2}P^y - -jkH_0 x . \tag{142}$$

Using the point matching method, equation (142) is reduced to the following set of equations that need to be solved to determine $\vec{M}_s$.

$$j\omega F_{ij}^{y} + \frac{1}{2}P_{ij}^{y} = -jkH_0 x_{ij} \,. \tag{143}$$

Equation (143) cannot be solved in this form as there are more variables than equations. F_{ij}^{y} depends on the magnetic surface currents, M_{ij}^{y}, and P_{ij}^{y} depends on the electric surface currents, J_{ij}^{x}. It is possible, however, to express the electric surface current in terms of the magnetic currents through the use of the auxilliary relationship that relates the tangential electric field to the electric surface current.

Assuming that the wires of the mesh lie along the x and y axes and that the incident magnetic field lies along the y-axis according to (23), then, following the procedure of Casey [34,35], it can be shown that the tangential electric field only has an x-component and that equation (64) reduces to the scalar equation

$$E^{x} = \frac{a_s^2}{j\omega C_s}\frac{\partial^2 J^{x}}{\partial x^2} \,. \tag{144}$$

Equation (144) can be re-written in finite difference form as

$$E_{ij}^{x} = \frac{a_s^2}{j\omega C_s}\frac{J_{i-1j}^{x} - 2J_{ij}^{x} + J_{i+1j}^{x}}{h^2} \tag{145}$$

or, alternatively, in matrix form as

$$\vec{E}^{x} = \ddot{A} \cdot \vec{J}^{x} \,. \tag{146}$$

The matrix, $\ddot{A}$, is sparse having elements only on or adjacent to the diagonal. Multiplication of both sides of (146) by the inverse of the matrix, $\ddot{A}$, yields the following equation for the electric surface current vector

$$J^x = \bar{A}^{-1} \cdot \vec{E}^x \tag{147}$$

Noting that $\vec{P}_s = \hat{z} \times \vec{J}_s$ and $\vec{M}_s = \hat{z} \times \vec{E}_t$ then equation (147) can be rewritten as

$$\vec{P}_s^y = \bar{A}^{-1} \cdot \vec{M}_s^y \tag{148}$$

Substitution of this relationship into (143) gives a set of equations only in terms of M_s^y which is then solvable.

Equation (143) was solved using the Method of Moments. The matrix, $\bar{A}$, was created from the finite difference expression (145) and then the inverse of this matrix was calculated using LINPACK matrix sub-routines. Finally, I assembled the complete Moment Method matrix and solved it to determine the electric insertion loss of the wire grids and meshes by comparing results for open and loaded apertures. Table 6 shows calculated values of the electric insertion loss for bonded and unbonded wire meshes and unidirectional grids.

As anticipated from Casey's theory, the calculated electric insertion loss was found to be independent of frequency.

Table 6 - Calculated Electric Insertion Loss for Wire Meshes and Grids

Number of Wires	Insertion Loss (dB) Bonded Mesh	Insertion Loss (dB) Unbonded Mesh	Insertion Loss (dB) Unidirectional Grid
1	5.40	5.40	3.20
3	9.42	9.42	6.13
7	14.96	14.96	10.66
15	21.98	21.98	16.88
31	30.48	30.48	24.85

Chapter 5:

Measurement of EM Penetration Through Open and Loaded Apertures

5.1 Introduction

The use of composite materials for the construction of aircraft and ships is becoming increasingly more common because of their superior specific strength and stiffness, flammability resistance and economic gains. A knowledge of the electromagnetic (EM) properties of these anisotropic laminated materials is necessary because of their limited conductivity and the increased susceptibility of modern electronic systems to electromagnetic pulse (EMP) and electromagnetic interference (EMI). The electromagnetic properties of composite materials have been the subject of a number [34-39] of experimental and analytical studies during the late 1970's and early 1980's. Optically transparent conductive films as well as wire grids and screens are often used to provide EM shielding to large apertures, such as windows in buildings, aircraft, and ships where visibility is needed.

This chapter presents the results of measurements that have been made to determine both the electric and magnetic shielding properties of carbon, non-carbon and hybrid fibre composite materials, as well as bonded and unbonded wire meshes and wire grids. The variables examined included, for the composite materials, the effects of fibre type, fibre conductivity and orientation, sample lay-up, degree of hybridization and contact resistance; and for the grids and meshes, the effect of wire spacing and mesh size. The present study was undertaken as a result of the development of new experimental techniques and new materials both of which are relevant to various current and future civilian and military systems.

5.2 Experimental Procedures

5.2.1 Composite Materials

The composite materials tested were multi-ply unidirectional or cross-plied epoxy matrix composite laminates containing carbon, glass, aramid and boron fibres. The samples were prepared by standard autoclaving procedures and consisted of six or eight-ply laminates. The unidirectional plies were arranged in various orientations (eg. 0°, ±45°, 90°). Table 7 shows the lay-ups of the samples used in these studies which were 18 cm square. Hybrid laminates were also produced by mixing fibres on a layer to layer basis.

Table 7 - Preparation of the Composite Samples

Fibre Material	Number of Plies	Sample Lay-Up
AS-4	8	0°
AS-4	8	30°
AS-4	8	45°
AS-4	8	±45°
AS-4	8	0°,±45°,90°
AS-4	6	0°,±60°
AS-4/Glass	2/AS-4 6/Glass	0° 0°
AS-1	8	0°
IM-6	8	0°
IM-7	8	0°
Boron	8	0°

5.2.2 Peparation of the Wire Meshes and Grids

To prepare samples to examine the effect of wire spacing on the shielding properties of wire meshes and screens, a square aluminum frame with an 18 cm outside dimension and a 14.5 cm inside dimension was drilled with 31 equally spaced holes. By stringing different numbers of #26 AWG copper wire onto this frame, unidirectional wire grids having 2, 4, 8, 16 and 32 equally spaced segments were constructed. By stringing wires in the two orthogonal directions, wire meshes having equal mesh size were made. To bond the mesh, the wire contacts were soldered and to form an unbonded mesh one set of wires was insulated using spaghetti tubing.

5.2.3 Electrical Contact

To obtain a proper measurement of the shielding properties of the composite samples, good electrical contact must exist between the sample and the body of the transverse electromagnetic (TEM) cell used to make the measurements. To achieve this, the edges of all of the samples were silver painted and then an aluminum gasket was attached to the painted edge of the sample again using silver paint. Finally, the gasket was painted onto the TEM cell surface. Pressure applied to the upper cell helped to ensure good contact between the two cells.

5.2.4 Measurement Techniques

(i) Dual TEM Cell

To make the EM shielding measurements, a dual TEM cell was used. In this method, two TEM cells are coupled by a common aperture as shown in Figure 15.

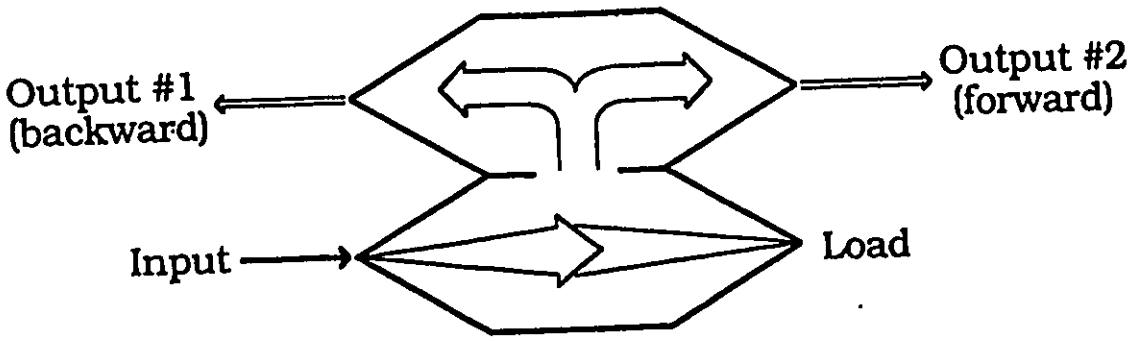

Figure 15 - Schematic Diagram of a Dual TEM Cell Showing EM Wave Penetration

Measurements are made of the penetration of the EM fields from the driven (lower) cell into the receiving (upper) cell. Insertion loss measurements are made by comparing the results when the aperture is loaded with a conductive sample with results for the open (unloaded) aperture.

The theory of the dual TEM cell has been developed by Wilson and Ma [9,40]. Provided the aperture dimension is small compared to the wavelength used, small aperture theory can be used and the penetration of the EM fields into the upper cell treated in terms of the equivalent electric and magnetic polarizabilities of the aperture. The output of the cell in the forward direction is related to the sum of the electric and magnetic polarizabilities. In the backwards direction it is related to the difference. Expressions for the forward and backward insertion losses (defined as the ratio of the transmitted power with material to that of an open aperture) are given below.

$$IL_{forward}=20\log\left|\frac{\alpha_{ey}+\alpha_{mx}}{a_{ey}+a_{mx}}\right| \tag{149}$$

and

$$IL_{backwards}=20\log\left|\frac{\alpha_{ey}-\alpha_{mx}}{a_{ey}-a_{mx}}\right| . \tag{150}$$

Experimentally it is possible to separate the electric and magnetic properties of the material by adding or subtracting the two outputs of the receiving cell using a hybrid junction [41] which gives;

$$IL_e=20\log\left|\frac{\alpha_{ey}}{a_{ey}}\right| \tag{151}$$

and

$$IL_m=20\log\left|\frac{\alpha_{mx}}{a_{mx}}\right| . \tag{152}$$

The dual TEM cell used in these studies was designed by Dr. S. Kashyap and built at the National Research Council of Canada.

(ii) Frequency Domain Measurements

Measurements of the magnetic and electric insertion loss of the laminates were made over the frequency range from 2 to 200 MHz using a Hewlett Packard HP8753B Network Analyzer. The outputs from the two ends of the receiving TEM cell were combined to give either the sum or difference signal using an Anzac Model HH-107 Hybrid Junction. The characteristics of the hybrid junction limited tha range of frequencies that could be measured. The TEM cell had the capability of making measurements to about 600 MHz before higher order modes were excited.

Values for the insertion loss were obtained by dividing the magnetic and electric shielding effectiveness data for the open aperture by the corresponding results for the aperture loaded with a conductive sample. Open aperture results were stored on disk and could be retrieved by the Network Analyzer.

(iii) Time Domain Measurements

A few shielding and insertion loss measurements have also been made in the time domain. In this case, a double exponential pulse was generated using an Analogic Model 2045 Arbitrary Function Generator and fed into the input of the lower TEM cell. The following equation shows the form of the pulse used

$$E(t) = 5.0 \times (e^{-\beta t} - e^{-\alpha t}) \quad Volts \tag{153}$$

where $\alpha = 4.76 \times 10^7\ s^{-1}$ and $\beta = 4.00 \times 10^6\ s^{-1}$

The two outputs from the receiving cell were combined in the hybrid junction to give either the sum or difference signal. This signal was then amplified using an EIN Model 411LN Broad Band Amplifier (100 kHz to 300 MHz bandwidth) that provided approximately 40 dB gain. The output was recorded on a Tektronix DSA602 Digitizing Signal Analyzer. The relatively fast fall time was used to minimize distortion of the output signal as a result of the limited low frequency response of the amplifier.

5.3 Experimental Results

5.3.1 Composite Materials

(i) Effect of Fibre Type

The effect of fibre type on the magnetic shielding properties of a number of different materials is shown below in Figure 16. Interestingly, the difference between three types of carbon fibre materials is not large (~5 dB). Various workers, including McMahon [42], have shown that fibre electrical resistivity decreases with increasing elastic modulus. The present carbon fibres have resistivities from approximately 19 $\mu\Omega$.m (AS1 & AS4) to 12 $\mu\Omega$.m (IM6 & IM7). According to the theory of loaded apertures developed by Casey [12,31] and Latham and Lee [30] this difference in fibre conductivity should translate logarithmically to the shielding characteristics (in dB). These higher modulus carbon fibres should therefore be the preferred reinforcement and the present results suggest such a trend. Even higher modulus carbon fibres exist such as P-100 from Union Carbide with a resistivity as low as 5 $\mu\Omega$.m. Clearly advantages may exist in mixing carbon fibre types to optimize shielding as well as mechanical properties.

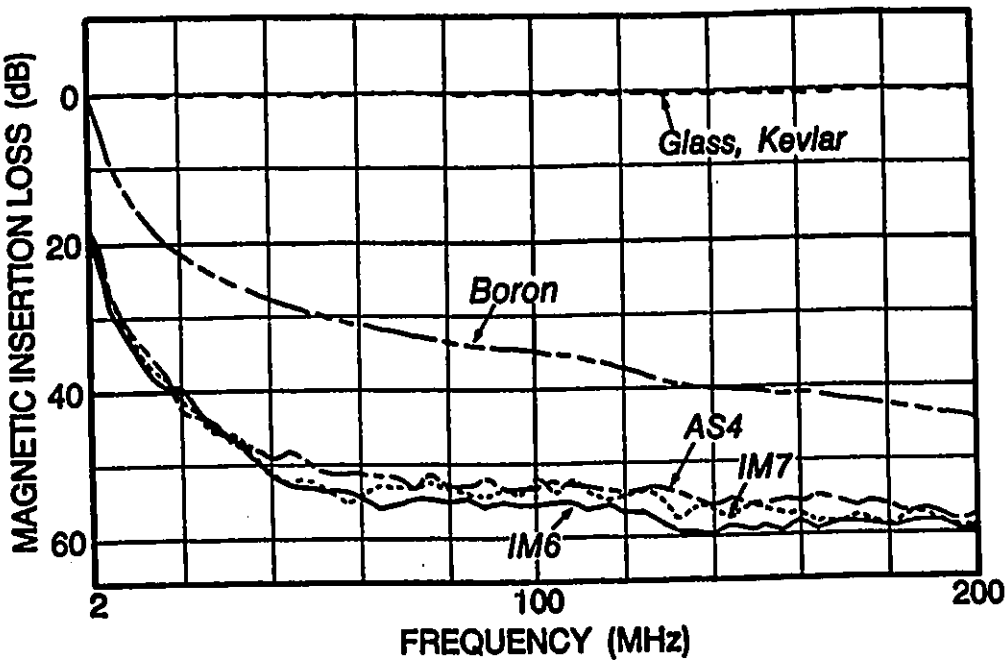

Figure 16 - Effect of Fibre Type on the Magnetic Insertion Loss of Composite Materials

As anticipated, the glass and aramid fibres provide essentially no shielding as they are non-conducting. The boron-epoxy sample on the other hand provides an intermediate degree of shielding as the central core of each fibre is a tungsten filament. This is consistent with conductivity measurements [36] on boron fibres.

(ii) Effect of Fibre Orientation

Fibre orientation has a major influence on magnetic shielding, as is seen in Figure 17, which shows the magnetic insertion loss of AS-4 carbon composite material having fibres oriented unidirectionally at 0°, 30°, 45°, 60° and 90° to the direction of propagation of the EM wave. The insertion loss measurements for the 0° sample are probably influenced by the limited dynamic range of the network analyzer.

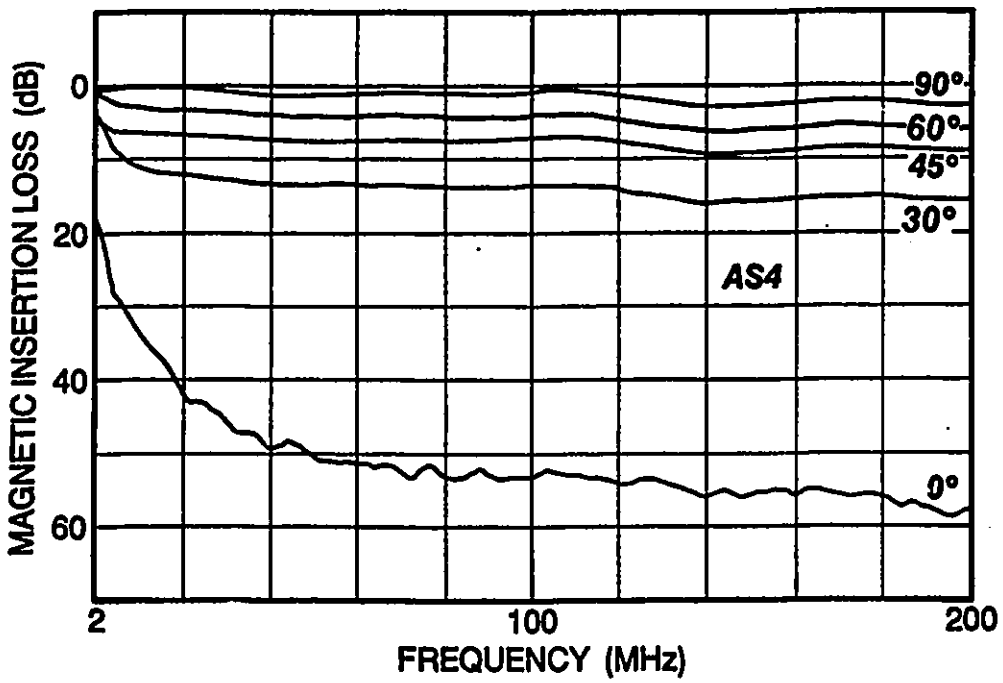

Figure 17 - Magnetic Insertion Loss of an 8-Ply, AS-4 Unidirectional Composite Material as a Function of Orientation.

Qualitatively these results relate directly to the anisotropic conductivity of the composite laminate. The conductivity is greatest along the fibres, and hence, when they are oriented at 0°, there is very little interruption of the current flow along the body of the cell and shielding is high. By comparison, the conductivity transverse to the fibres is lowest leading to poor shielding when the fibres are oriented at 90°.

The numerical results presented earlier are in good qualitative agreement with the experimental results shown above. These results were calculated assuming that the resistance in the direction normal to the fibres was infinite (ie $\sigma_{yy} = 0$). In reality there is sufficient contact between neighbouring fibres to provide limited conductivity in the direction orthogonal to the fibre axis.

Figure 18 shows results for the measurement of the electric insertion loss of unidirectional AS-4 samples as a function of fibre orientation. These results appear to indicate that the electrical insertion loss is orientation dependent. Qualitatively, since the electrical penetration depends only on the normal component of the electric field, the electric insertion loss is expected to be independent of orientation. The theory presented in section 2.5.2.2 also predicts that the electrical shielding should be independent of orientation. The experimental results are thought to be influenced by the limited isolation (approximately 30 dB) between the two ports of the hybrid junction. When the magnetic signal is very large, it is thought that there is some leakage of the magnetic signal into the electric signal.

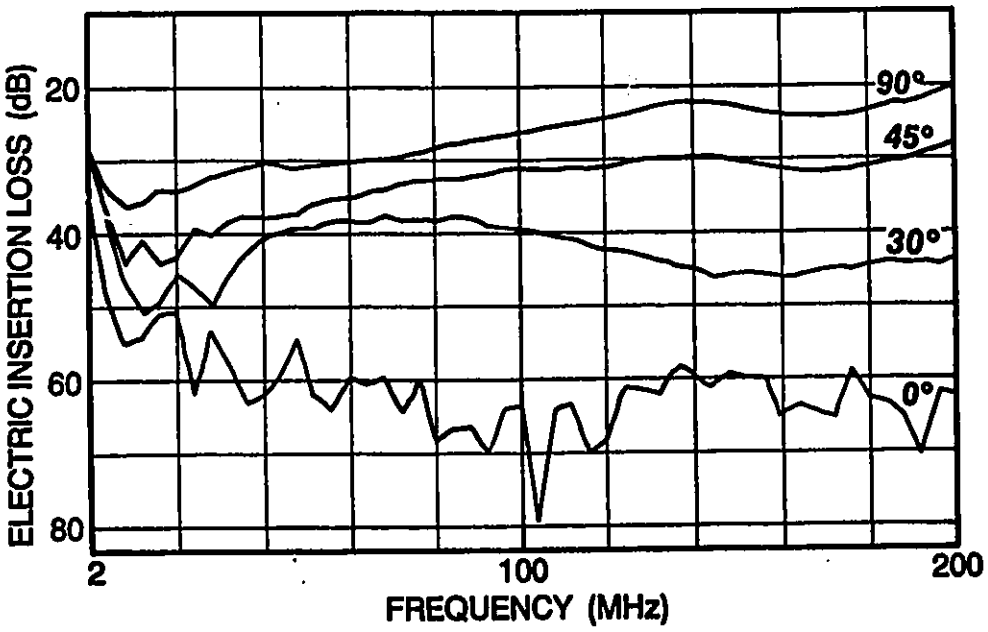

Figure 18 - Electric Insertion Loss of an 8-Ply, AS-4 Unidirectional Composite Material as a Function of Orientation.

Measurement of the electrical shielding properties of the carbon composite samples is limited by the dynamic range of the Network Analyzer especially at the lower frequencies and for the 0° samples. The actual loss is probably higher than the loss measured under these conditions.

Because of the difficulty in making electric shielding measurements on unidirectional 0° and multidirectional samples with high insertion loss, most of the remaining discussion will concentrate on the magnetic properties of the laminates.

(iii) Effect of Lay-Up and Hybridization

Figure 19 compares the magnetic insertion loss for a number of laminates. This figure shows the effects of degree of hybridization and lay-up. The insertion loss follows the expected trend in sample conductivity. Thus, for example, the insertion loss from 8 layers of carbon fibre (AS-4/0°) is 8-14 dB higher (depending on frequency) than the AS-4/GLASS sample which contains two layers of 0° AS-4 fibre. From simple considerations, one might expect a difference of 12 dB based on sample conductivity.

Since 0° fibres provide high shielding, qualitatively the AS-4/0°, ±60° laminate (which contains two layers of 0° oriented fibre) should provide somewhat higher shielding than the AS-4/GLASS laminate as observed. Interestingly, in a ±45° pair of plies, the plies are orthogonal to each other. This suggests that a ±45° pair should have roughly the same shielding effectiveness as a single 0° oriented ply. On this basis, the insertion loss of the AS-4/±45° and AS-4/0°, ±45°,90° laminates are expected to lie between the curves for

AS-4/Glass and AS-4/0°. While this is true for low frequencies, the AS-4/±45° curve crosses the AS-4/0° at high frequencies. Two factors may account for this. Firstly the 0° sample is sensitive to slight misorientation and, secondly, for high loss samples the magnetic insertion loss measurements may be affected by the dynamic range of the instrument. It was noticed that the background noise level can vary from day to day.

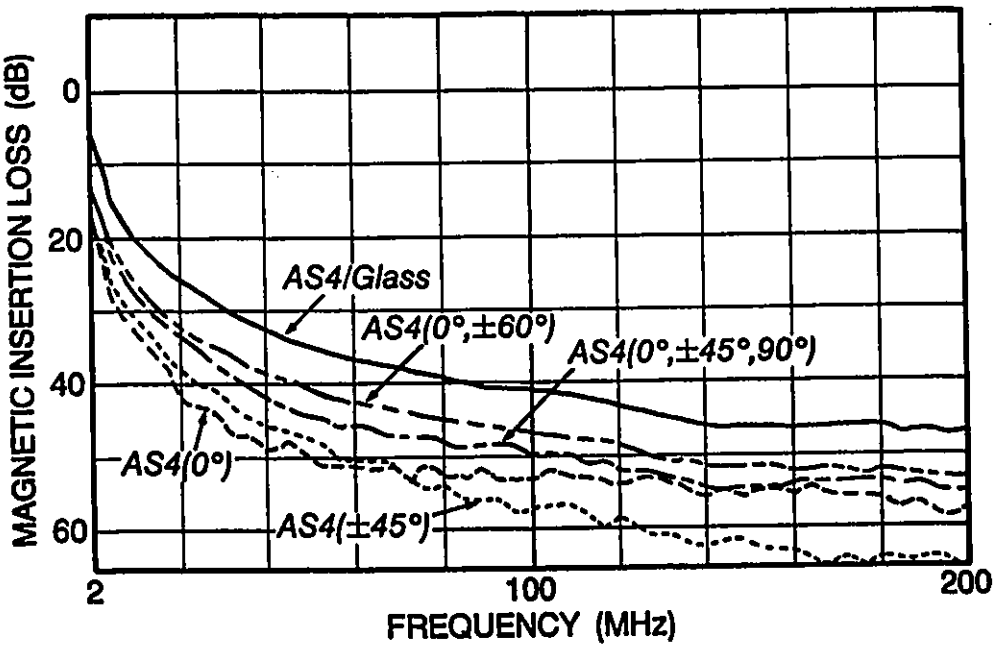

Figure 19 - The Effect of Sample Lay-Up on Magnetic Insertion Loss

A simple mathematical model that predicts the shielding properties of samples with multi-directional plies can be developed in the following way. Firstly, single ply attenuation factors, $\eta_{\parallel}$ *and* $\eta_{\perp}$, are derived from the experimentally measured magnetic insertion loss data for the 0° and 90° samples. Once these values are

determined, the transmitted field, H_{trans}, for a single ply can be written

$$H_{trans} = \sqrt{H_{\parallel}^2 + H_{\perp}^2} \tag{154}$$

where

$$H_{\parallel} = \cos^2\theta \times \eta_{\parallel} \qquad and \qquad H_{\perp} = \sin^2\theta \times \eta_{\perp} \tag{155}$$

For multilayer samples, resistivity is calculated by considering the layers to be connected in parallel electrically. A comparison between experimental values and values calculated using this model for 200 MHz is shown in Figure 20.

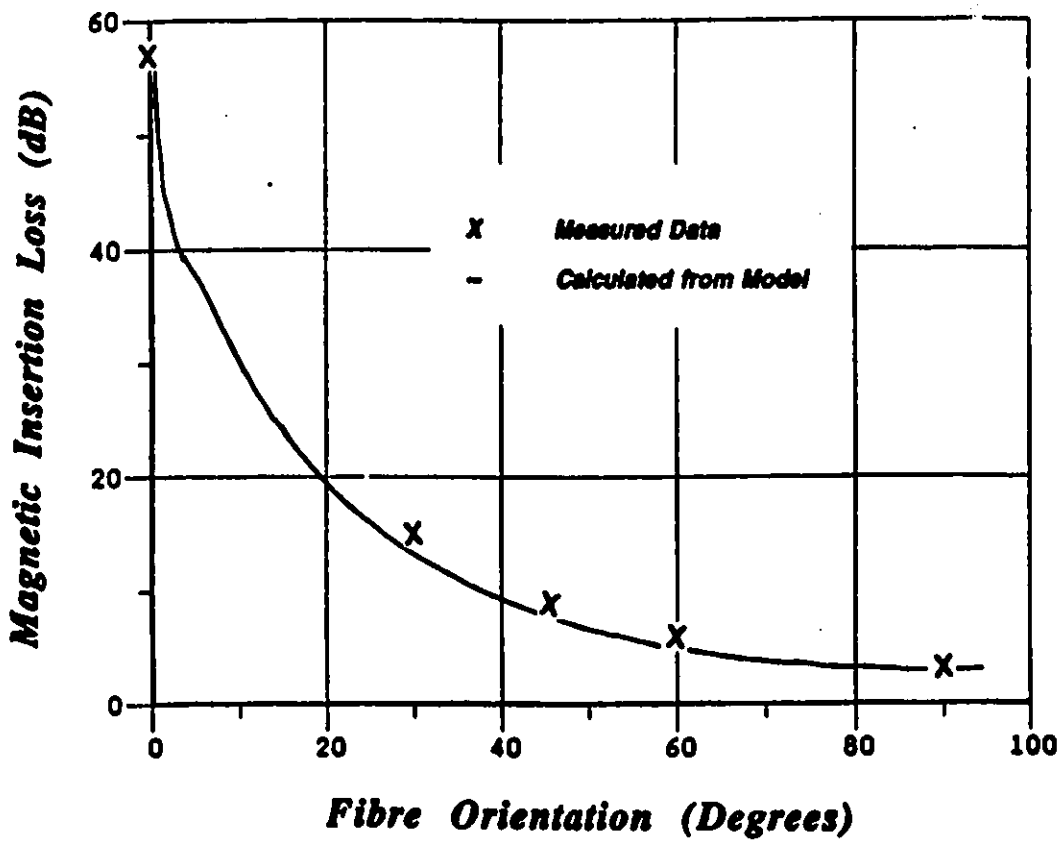

Figure 20 - Comparison of Experimental and Calculated Insertion Loss for Unidirectional AS-4 Samples as a Function of Orientation.

Table 8 includes estimates of insertion loss for the multidirectional laminates based on the model described previously.

Table 8 - Comparison of Measured and Calculated Insertion Loss (200 MHz)

Sample Lay-Up	Experimental Loss (dB)	Calculated Loss (dB)
AS-4/0°	56.9	-
AS-4/90°	3.0	-
AS-4/30°	15.4	7.8
AS-4/45°	9.0	5.4
AS-4/60°	6.2	4.0
AS-4/±45°	66.0	47.9
AS-4/0°,±45°,90°	55.0	49.3
AS-4/Glass	48.0	44.9
AS-4/0°,±60°	53.0	39.3

(iv) Effect of Contact Resistance on Measurement of Shielding Properties

The three curves in Figure 21 show the effects of different methods of bonding the AS-4/0° composite sample to the body of the TEM cell on the magnetic insertion loss. The methods of bonding the sample to the TEM cell body were, from top to bottom;

a) use of a pressure contact.

b) use of copper tape to bond the laminate to the cell.

c) use of a metal gasket which was silver painted to both the laminate and cell.

In all cases, a coating of silver paint at the edge of the laminate ensured a good electrical contact with the end of the carbon fibres.

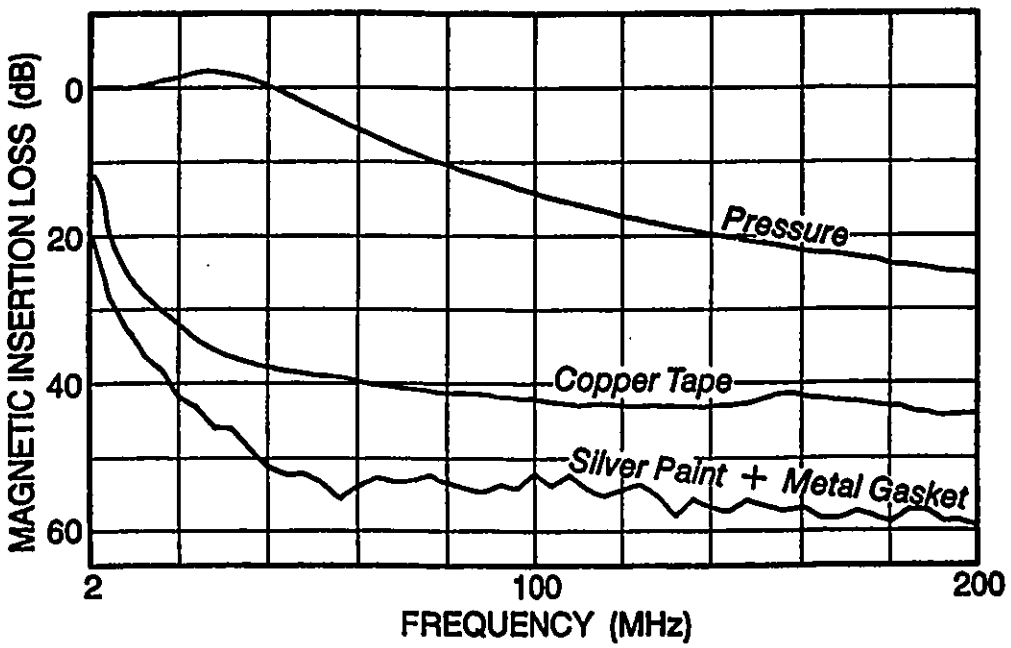

Figure 21 - The Effect of Contact Resistance on Magnetic Insertion Loss

These results show clearly the importance of making a good electrical contact with the sample if the shielding properties are not to be degraded. From a practical point of view, attention must be paid to forming low resistance joints when composite panels are joined (for example in aircraft or ship construction) if good shielding is to be maintained. Strawe [39] noted these effects previously.

The theory of the effect of contact resistance on shielding effectiveness has been further discussed by Casey [12]. To obtain reliable results, the contact resistance must be small compared to the sample resistance.

(v) Time Domain Measurements

Figure 22 shows time domain measurements of the magnetic shielding effectiveness of a unidirectional AS-4 sample oriented in the 0° and 90° directions. This Figure shows the output from the upper TEM cell in response to a double exponential pulse. These measurements represent total shielding effectiveness and include the attenuation effects of the aperture.

As anticipated from the frequency domain measurements, the amplitude of the time domain output pulse is much higher when the laminate is oriented in the 0° direction than in the 90° direction. The shape of the output pulse is different for the two orientations. This effect is important in determining coupling to equipment (for example to cables inside an aircraft or bridge of a ship).

The frequency domain results for the insertion loss of the open and loaded apertures explain the difference in shape of the output pulse for the two orientations. When the sample is oriented at 90°, the shielding effectiveness is dominated by the shielding of the aperture. The attenuation of the open aperture depends [9] inversely on frequency which results in a differentiation of the input pulse. When the laminate is oriented at 0°, the contribution the laminate makes is directly proportional to frequency and the total shielding is essentially frequency independent. Thus while the total signal is attenuated, the output signal shape remains essentially the same as the

input pulse.

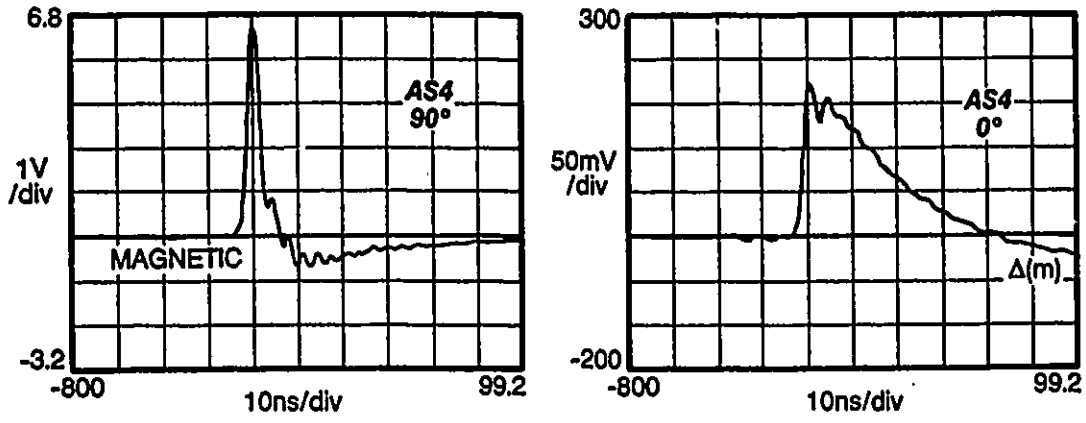

Figure 22 - Time Domain Measurement of Magnetic Shielding

5.3.2 Wire Meshes and Grids

The electric and magnetic shielding properties of the wire meshes and grids examined are similar and the experimental results can be presented together. Figures 23 and 24 show results for the magnetic insertion loss and electric insertion loss of a wire grid oriented so the wires lie along the direction of EM wave propagation for various numbers of wires. These results show that both the magnetic and electric insertion loss is essentially independent of frequency. This behaviour was also found for the bonded and unbonded wire meshes and is consistent with the theory of Casey [12] and that presented in section 2.5.2.

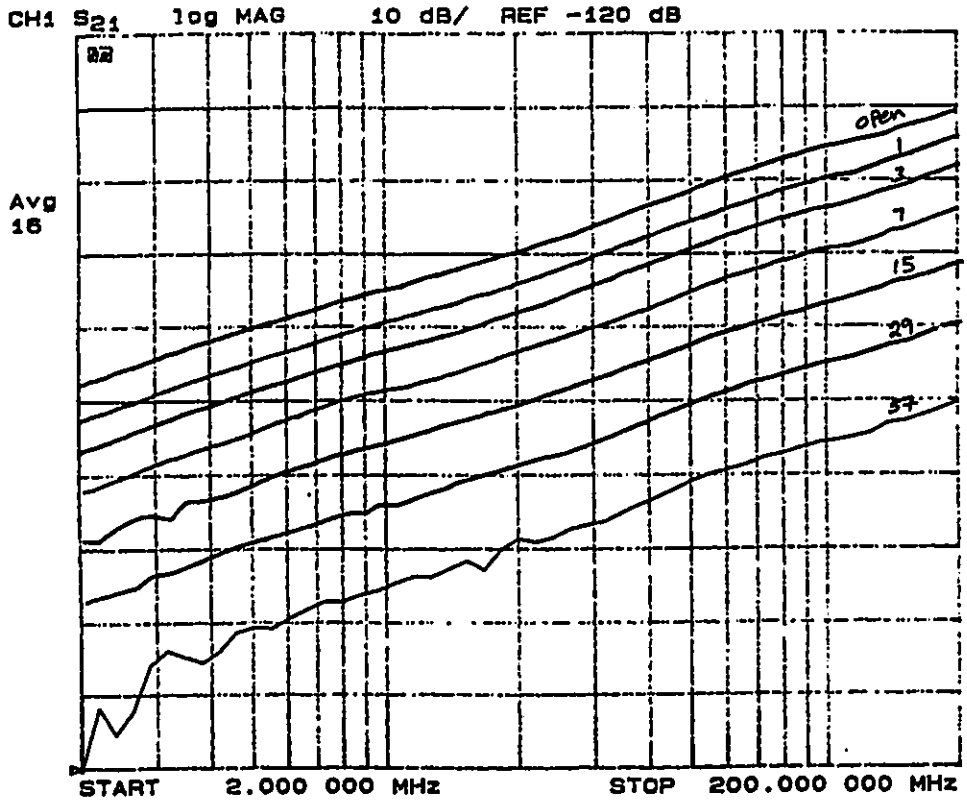

Figure 23 - Magnetic Shielding Effectiveness of Unidirectional Wire Grids

Tables 9 and 10 give values for the magnetic and electric insertion loss for all of the meshes and grids examined in this work. The following points are of particular interest;

a) The unidirectional wire grid provides no magnetic shielding when the wires are oriented perpendicular ($\theta = 90°$) to the direction of propagation. This behaviour is anticipated from the theory presented in section 2.5.2.4.

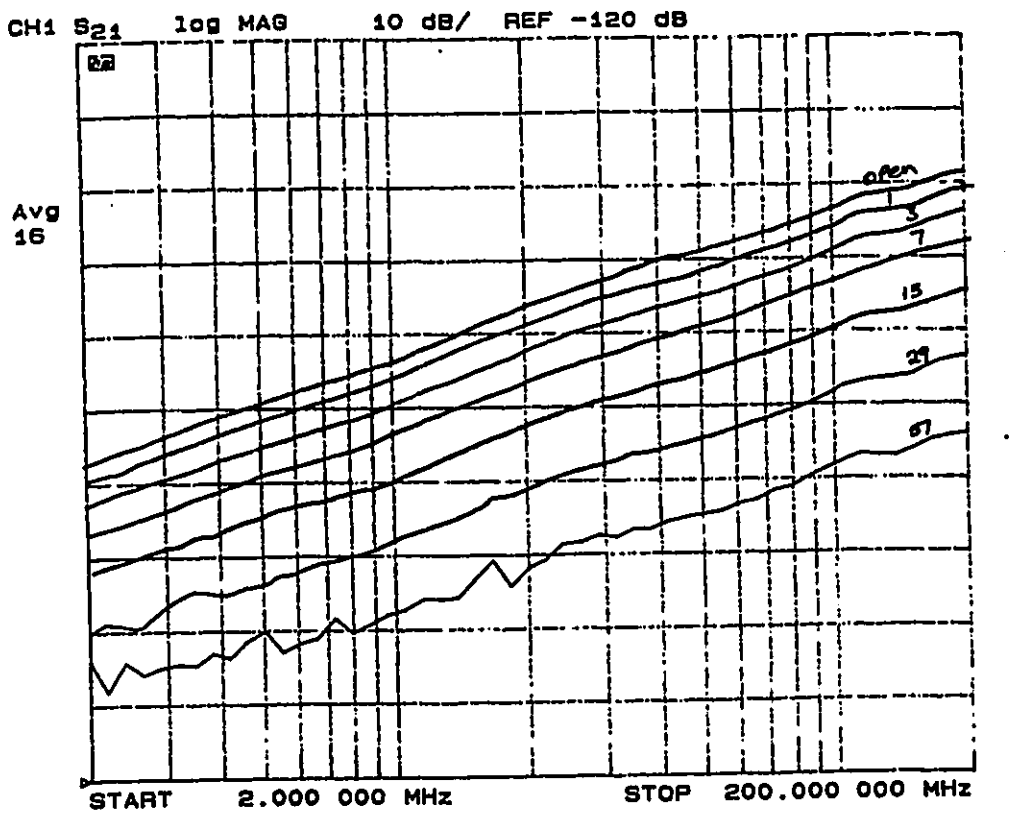

Figure 24 - Electric Shielding Effectiveness of Unidirectional Wire Grids

b) The electric shielding provided by the wire grids is independent of wire orientation.

c) The magnetic shielding provided by the bonded and unbonded wire meshes as well as the wire grids with $\theta = 0°$ is the same for equal numbers of parallel wires.

d) The electric shielding of the bonded and unbonded wire meshes is the same but higher than that provided by the equivalent wire grid. At high frequencies this difference amounts to a factor of two (6 dB).

Table 9 - Magnetic Insertion Loss of Wire Grids and Meshes

# of Wires	Magnetic Insertion Loss			
	Wire Grid ($\theta = 0°$)	Wire Grid ($\theta = 90°$)	Wire Mesh ($Z_c = 0$)	Wire Mesh ($Z_c = \infty$)
1	3.82	0	3.87	4.01
3	8.64	0	8.50	8.43
72	14.73	0	14.61	14.46
15	22.03	0	22.58	21.99
31	31.09	0	-	30.96

Table 10 - Electric Insertion Loss of Wire Grids and Meshes

# of Wires	Electric Insertion Loss			
	Wire Grid ($\theta = 0°$)	Wire Grid ($\theta = 90°$)	Wire Mesh ($Z_c = 0$)	Wire Mesh ($Z_c = \infty$)
1	2.09	2.09	3.88	4.16
3	5.45	5.45	8.89	9.52
7	10.16	10.16	15.34	17.79
15	16.78	16.49	24.16	23.64
31	25.49	25.49	-	34.68

Chapter 6
Conclusions

In the theoretical portion of this work, appropriate integro-differential equations have been derived for the determination of the equivalent magnetic surface currents on small apertures loaded with a variety of conductive materials of practical interest. The materials investigated include isotropic and anisotropic resistive sheets, and wire grids and meshes.

Numerical solution of these equations was accomplished using the Method of Moments. Equivalent magnetic and electric polarizabilities have been calculated for a square aperture loaded with the materials mentioned above. The numerical results are in good agreement with existing theoretical and numerical results as well as the results presented in the experimental portion of this thesis. Based on these theoretical and numerical results, I have reached the following conclusions:

a) When a resistive material is used to load the aperture, the magnetic insertion loss has the following form

$$IL_m = 20\log\left|1 + \frac{j\omega\sigma_s}{K}\right|$$

where K is a constant. This shows that the (absolute) insertion loss is linearly dependent on frequency (or alternatively the insertion loss in dB is dependent on log frequency) when the conductivity is high and the second term dominates. This means that resistive materials provide little shielding at low frequencies but are good at high frequencies. For poorly conducting materials

the first term dominates and the insertion loss is close to zero. The open aperture, on the other hand, acts as a high pass filter and provides good shielding at low frequencies. When the two effects are combined, a small aperture loaded with a resistive material has a magnetic shielding effectiveness that is almost independent of frequency. In the time domain, this means that an incident pulse is attenuated but its wave shape not significantly changed.

b) When a resistive material is used to load an aperture, the electric insertion loss has the form

$$IL_e = 20\log\left|1 + \frac{j\sigma}{\omega K}\right|$$

This shows that the (absolute) electric insertion loss is inversely dependent on frequency when the conductivity of the material is high and the second term dominates. For poorly conductive materials, the insertion loss is zero. The derivation of an appropriate expression for the electric insertion loss over the range of conductivities and frequencies has not been reported previously as far as the author is aware. Results given by Wilson and Ma [40] and by Gobin et al [32] appear to only be valid for highly conductive materials. At low frequencies the electric insertion loss is high and electric field penetration is generally not significant.

c) Both the electric and magnetic insertion losses of the wire grids and wire meshes are independent of frequency over the range of frequencies and spacings examined in this work. From a practical point of view, this means that an aperture loaded with a mesh or grid retains the characteristics of a high pass filter.

The dual TEM cell technique has been shown to be a valuable method to measure the magnetic and electric insertion loss of conductive materials.

With the composite materials, fibre type, fibre orientation, sample lay-up and contact resistance were found to control the EM loss characteristics. While carbon fibres have resistivities approximately 3 orders of magnitude higher than good metallic conductors (Al, Cu and Ni), they do possess adequate conductivity to provide a substantial shielding to advanced composite structures. However other common reinforcements such as aramid and glass fibres are incapable of providing adequate shielding unless mixed (hybridised) with carbon fibres. The highest modulus fibres are the preferred reinforcement from the standpoint of maximizing shielding. Fibre orientation has a major influence on both the magnetic and electric shielding properties of samples having only unidirectional fibres but multidirectional laminates experience less severe orientation effects. The results show the major importance of obtaining a low resistance contact with the ends of the carbon fibres when composite panels are connected if the intrinsic material shielding properties are to be maintained.

With the wire meshes and grids, I found that, when wires with good conductivity are used, the reactive component of the surface impedance dominates. This results in electric and magnetic insertion losses that are independent of frequency. When at least one set of wires lies along the direction of propagation, the magnetic shielding provided by the meshes, and a wire grid is the same when the same numbers of wires (in a given direction) are used. Based on the results of Kontorovich [13], the shielding properties of the bonded and unbonded meshes are expected to be different for an arbitrary angle of incidence of the EM wave. The electric shielding of the wire meshes was found to be greater than the wire grid for an equal number of wires.

Chapter 7

References

1. EMP Engineering and Design Principles, Bell Telephone Laboratories, Whippany, New Jersey, 1975.

2. C.D. Taylor and N.H. Younan, "Effects from High Power Microwave Illumination", Microwave Journal, June 1992, p. 80.

3. H.W. Ott, Noise Reduction Techniques in Electronic Systems, John Wiley and Sons, 1988. Chapter 6.

4. R.F. Harrington, Time Harmonic Electromagnetic Fields, McGraw-Hill Book Company, New York, 1961. p. 106.

5. J. van Bladel and C.M. Butler, "Aperture Problems", Proc. NATO Adv. Study Inst. on Theoretical Methods for Determining the Interaction of Electromagnetic Waves with Structures, J. Skwirzynski, Ed., Sythoff and Noordhoff International Publishers, 1979.

6. C.M. Butler, Y. Rahmat-Samii and R. Mittra, "Electromagnetic Penetration Through Apertures in Conducting Surfaces", IEEE Trans. on Antennas and Propagation, AP-26, 82 (1978).

7. R.E. Collin, Field Theory of Guided Waves, IEEE Press, New York, 1991.

8. J.D. Jackson, Classical Electrodynamics, John Wiley and Sons, New York, 1952.

9. P.F. Wilson and M.T. Ma, "Shielding Effectiveness Measurements with a Dual TEM Cell", IEEE Trans. on Electromagnetic Compatibility, EMC-27, 137 (1985).

10. A.F. Stevenson, "Solution of Electromagnetic Scattering Problems as a Power series in the Ratio (Dimensions Scatterer/Wavelength)", J. Appl. Phys., 24, 1134 (1953).

11. J.A. Stratton, Electromagnetic Theory, McGraw-Hill Book Co., New York, 1941.

12. K.F. Casey, "Low-Frequency Electromagnetic Penetration of Loaded Apertures", IEEE Trans. on Electromagnetic Compatibility, EMC-23, 367 (1981).

13. M.I. Kontorovich, "Averaged Boundary Conditions at the Surface of a Grating with Square Mesh", Radio Engineering and Electronic Physics, 8, 1446 (1963).

14. D. Kajfez, "Multiconductor Transmission Lines", AFWL Interaction Note # 151, June 1972.

15. J.R. Wait, "Theories of Scattering from Wire Grid and Mesh Structures", Electromagnetic Scattering, Academic Press, 1978.

16. M.I. Kontorovich, V.Yu. Petrunkin, N.A. Yesepkina, and M.I. Astrakhan, "The Coefficient of Reflection of a Plane Wave from a Plane Wire Mesh", Radio Engineering and Electronic Physics, 2, 222 (1962).

17. C.J. Bouwkamp, "Diffraction Theory", Rep. Prog. Phys., 17, 35 (1954).

18. C.J. Bouwkamp, "Theoretical and Numerical Treatment of Diffraction Through a Circular Aperture", IEEE Trans. on Antennas and Propagation, AP-18, 152 (1970).

19. H.A. Bethe, "Theory of Diffraction by Small Holes", Phys. Rev., 66, 163, (1944).

20. S.B. Cohn, "Determination of Aperture Parameters by Electrolytic Tank Measurements", Proc. IRE, 39, 1416 (1951).

21. S.B. Cohn, "The Electric Polarizability of Apertures of Arbitrary Shape", Proc. IRE, 40, 1069 (1952).

22. F. de Meulenaere and J. van Bladel, "Polarizability of Some Small Apertures", IEEE Trans. on Antennas and Propagation, AP-25, 198 (1977).

23. C.M. Butler, "Formulation of Integral Equations for an Electrically Small Aperture in a Conducting Screen", AFWL Interaction Note # 149, December, 1973.

24. Y. Rahmat-Samii and R. Mittra, "Electromagnetic Coupling Through Small Apertures in a Conducting Screen", IEEE Trans. on Antennas and Propagation, AP-25, 180 (1977).

25. R.F. Harrington and J.R. Mautz, "A Generalized Network Formulation for Aperture Problems", IEEE Trans. on Antennas and Propagation, AP-24, 870, (1976).

26. J.R. Mautz and R.F. Harrington, "Electromagnetic Transmission Through a Rectangular Aperture in a Perfectly Conducting Plane", Report # AFCRL-TR-76-0056, 1976.

27. R.F. Harrington and J.R. Mautz, "A Generalized Network Formulation for Aperture Problems", Report # AFCRL-TR-75-0589, 1975.

28. J.R. Mosig, "Integral Equation Technique", Numerical Techniques for Microwave and Millimeter-Wave Passive Structures, T. Itoh, Ed., John Wiley and Sons, 1989.

29. D.R. Wilton and A.W. Glisson, "On Improving the Stability of Electric Field Integral Equation at Low Frequency", IEEE AP-S Int. Symp., Los Angeles, CA., June 1981.

30. R.W. Latham and K.H.S. Lee, "Magnetic Field Leakage into a Semi-Infinite Pipe", Can. J Phys., 46, 1455 (1968)

31. K.F. Casey, "Electromagnetic Shielding Behaviour of Wire-Mesh Screens", IEEE Trans. EMC, 30, 298 (1988).

32. V. Gobin, J.C. Alliot and P. Degauque, "Modelling of Electromagnetic Wave Penetration Through Loaded Apertures", Int. J. Numerical Modelling, 4, 163 (1991).

33. A.W. Glisson and D.R. Wilton, "Simple and Efficient Numerical Methods for Problems of Electromagnetic Radiation and Scattering from Surfaces", IEEE Trans. Antennas and Propagation, AP-28, 593 (1980).

34. K.F. Casey, "EMP Penetration Through Advanced Composite Skin Panels", AFWL Interaction Note 315, December, 1976.

35. K.F. Casey, "Electromagnetic Shielding by Advanced Composite Materials", AFWL Interaction Note 341, June 1977.

36. Electromagnetic Effects of (Carbon) Composite Materials upon Avionic Systems, AGARD Conference Preprint 283, June 1980.

37. J.L. Allen, "Electromagnetic Shielding Effectiveness for Isotropic and Anisotropic Materials", RADC-TR-81-162 (1981).

38. A.T. Adams et al, "Electromagnetic Properties and Effects of Advanced Composite Materials: Measurement and Modeling", RADC-TR-78-156 (1978).

39. D. Strawe and L. Piszker, "Interaction of Advanced Composites with Electromagnetic Pulse Environment", RADC TR-75-141 (1975).

40. P.F. Wilson and M.T. Ma, "Techniques for Measuring the Electromagnetic Shielding Effectiveness of Materials: Part II-Near-Field Source Simulation", IEEE Trans. EMC, 30, 251 (1988).

41. D.F. Higgins, R. Wheeler and E. Wenaas, "A Comparison of Theoretical and Experimental Data for EM Penetration Through Small Apertures", IEEE Trans. Nuclear Sci., 32, 4340 (1985).

42. P.E. McMahon, ASTM STP 521,pp 367-389 (1973).

Appendix 1

Solution of Van Bladel's Equation Using the Finite Difference Method

Introduction

It is well known [19] that a small aperture in a plane conducting screen radiates like a combination of an electric and a magnetic dipole. The theory of small apertures has been developed by van Bladel and Butler [5] using an integro-differential equation approach.

Van Bladel and Butler have shown that the equivalent electric dipole moment, $\vec{p}_e$,for a small aperture is given by

$$\vec{p}_e = 2E_z^i\sqrt{S}e_0\iint\tau_0 ds = 2E_z^i S^{\frac{3}{2}}e_0(\tau_0)_{avg} \qquad (1)$$

where E_z^i is the normal component of the incident field, S is the aperture surface area and τ_0 is a solution of the following normalised equation.

$$\nabla_t^2\frac{1}{2\pi}\iint_A\frac{\tau_0(r')}{|r-r'|}ds' = -\frac{1}{\sqrt{S}} \quad . \qquad (2)$$

τ_0 is zero on the aperture boundary.

Solution Using the Finite Difference Method

The square aperture is divided into n x n segments as shown in Figure 1.

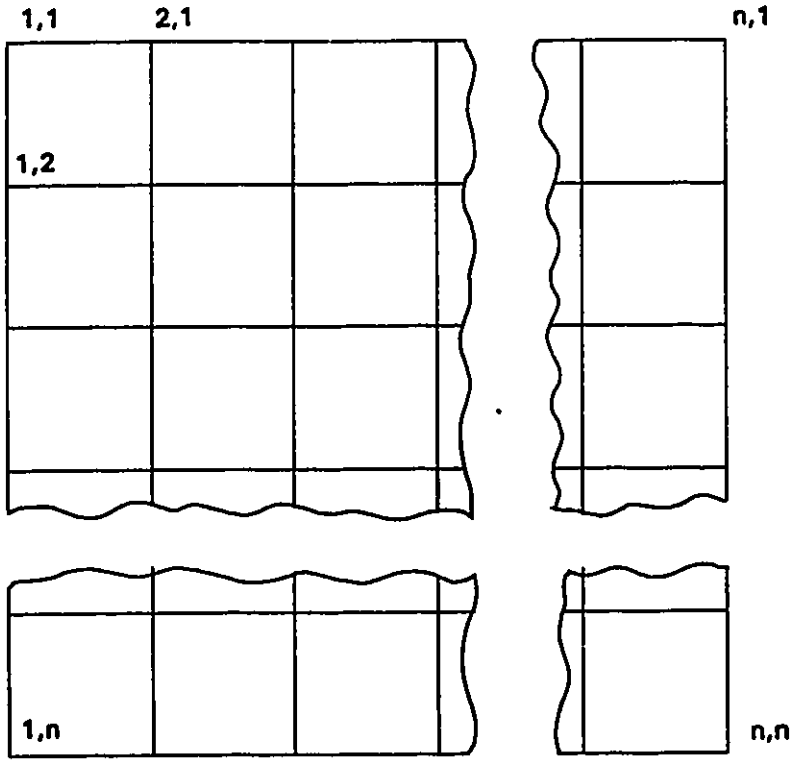

Figure 1 - Subdivision of the Square Aperture into Segments

If the auxilliary function

$$F(x,y) = \iint_A \frac{\tau_0(r')}{|r - r'|} ds' \tag{3}$$

is defined, then equation (2) can be rewritten in the form

$$\nabla^2_{x,y} F(x,y) = \frac{-2\pi}{\sqrt{S}} \quad . \tag{4}$$

Using the five point difference operator for the node i,j, the above equation can be rewritten in the form

$$\frac{F_{i-1,j} + F_{i+1,j} + F_{i,j-1} + F_{i,j+1} - 4F_{i,j}}{h^2} = \frac{-2\pi}{\sqrt{S}} \quad . \tag{5}$$

If h = 1 and i,j = 1,...n then $\sqrt{S} = n-1$ (ie. the length of the side of the aperture is n-1).

If the assumption is made that τ_0 is constant over each cell (of area h^2) of the aperture and that the distance between the source and observation point can be considered constant, then equation (3) can be written as

$$F(x_i,y_j) = F_{i,j} = \sum_{k=1}^{n}\sum_{l=1}^{n} \frac{\tau_0(k,l)}{\sqrt{(i-k)^2 + (j-l)^2}} \quad . \tag{6}$$

When k = i and l = j, this approximation is not not valid as a singularity occurs. Considering a circular region of radius, a, surrounding the observation point, then

$$\int_0^a \int_0^{2\pi} \frac{ds}{R} = \int_0^a \int_0^{2\pi} \frac{RdRd\theta}{R} = 2\pi a \quad . \tag{7}$$

By equating equivalent area of integration, it is found that $a = 1/\sqrt{\pi}$. Equation (6) is then given by

$$F(i,j) = \left(\sum_{k=2}^{n-1}\sum_{l=2}^{n-1} \frac{\tau(k,l)}{\sqrt{(i-k)^2 + (l-j)^2}}\right)_{k,l\neq i,j} + 3.54\tau(i,j) \, . \tag{7}$$

It should be noted that the summation has not been carried out over the nodes on the boundary since $\tau_0 = 0$ on the boundary.

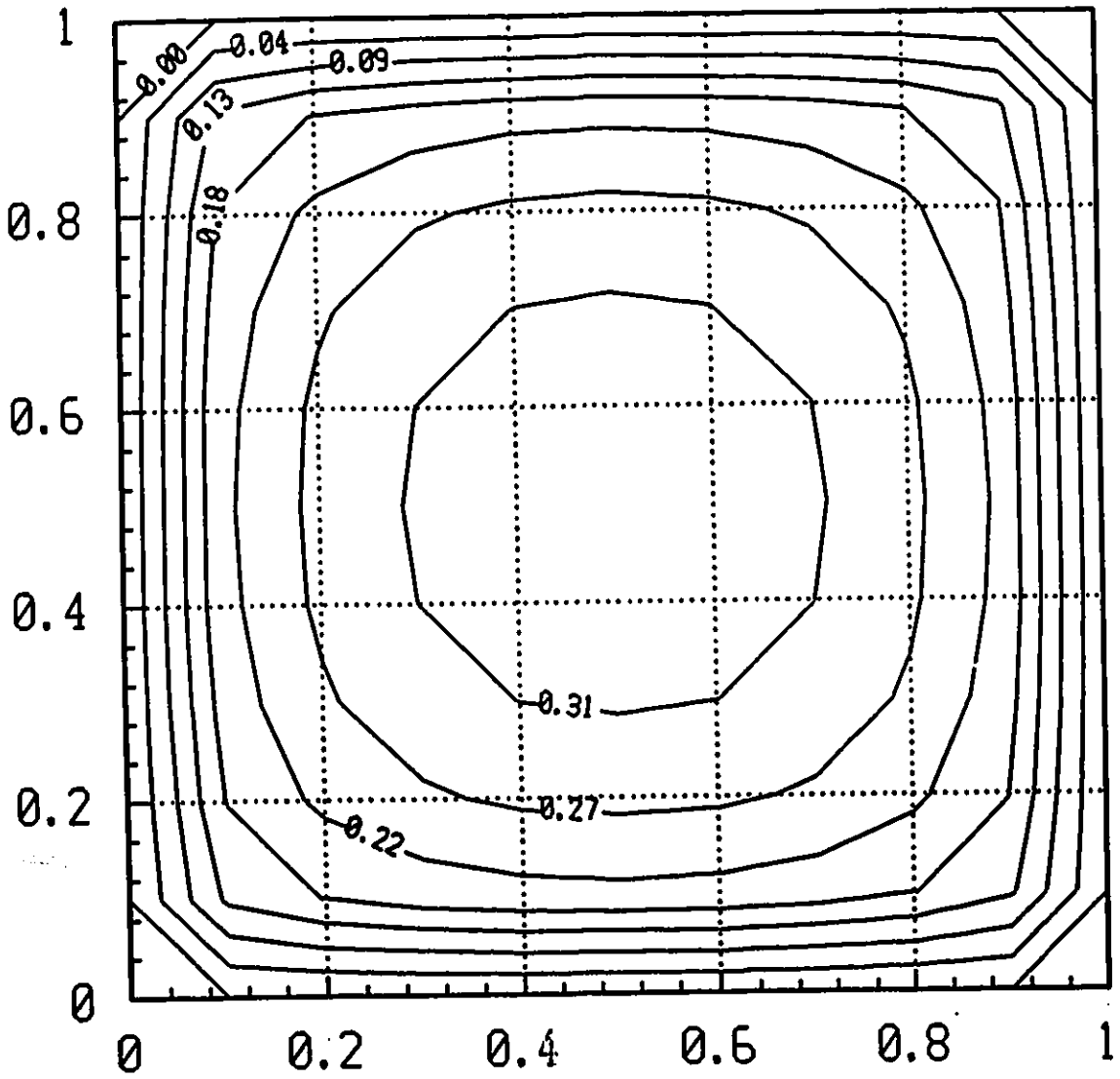

Figure 2 - Variation of τ_0 in a Square Aperture

If $G(k,l) = \sqrt{k^2 + l^2}$ but $G(0,0) = 1/3.54$ then equation (8) can be rewritten as

$$\sum_{k=2}^{n-1} \sum_{l=2}^{n-1} C_{k,l}^{ij} \tau_0(k,l) = \frac{-2\pi}{\sqrt{S}} \tag{9}$$

where

$$C_{k,l}^{ij} = \left[\frac{1}{G_{k-i-1,j-l}} + \frac{1}{G_{k-i+1,j-l}} + \frac{1}{G_{k-i,j-l-1}} + \frac{1}{G_{k-i,j-l+1}} - \frac{4}{G_{k-i,j-l}}\right] . \tag{10}$$

A computer to solve this system of equation has been written. Contours of τ_0 in a square aperture using 11 segments are shown in Figure 2. These results are in general agreement with the results of de Meulenaere and van Bladel [22] which are shown below.

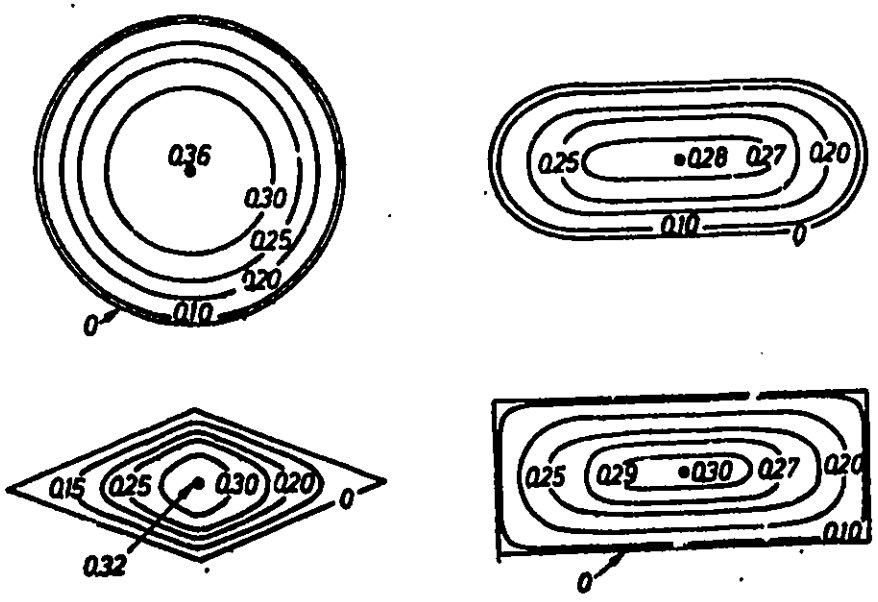

Figure 3 - Variation of τ_0 for some Aperture Cross Sections [22]

Appendix 2

Solution of Van Bladel's Equation Using the Method of Moments

Introduction

Van Bladel and Butler [5] have shown that the equivalent magnetic dipole moment, $\vec{p}_m$, of a small aperture is given by

$$\vec{p}_m = -2\iint_A (\vec{\rho}\cdot\vec{H}_t^i)\vec{r}\,ds \tag{1}$$

where the dimensionless vector, $\vec{\rho} = \hat{x}\rho_x + \hat{y}\rho_y$, is a solution of the following integro-differential equations

$$\frac{1}{2\pi}\nabla_t\iint_A \frac{\rho_x(x',y')\,ds'}{\sqrt{(x-x')^2+(y-y')^2}} = \hat{x} \tag{2}$$

and

$$\frac{1}{2\pi}\nabla_t\iint_A \frac{\rho_y(x',y')\,ds'}{\sqrt{(x-x')^2+(y-y')^2}} = \hat{y}\ . \tag{3}$$

For a square aperture, the problem reduces to the solution of equation (2) subject to the additional constraint

$$\iint_A \rho_x(x',y')\,ds' = 0\ . \tag{4}$$

Solution Using the Method of Moments

By writing $\nabla_t = \hat{x}\frac{\partial}{\partial x} + \hat{y}\frac{\partial}{\partial y}$, equation (2) can be reduced to the scalar equation

$$\frac{1}{2\pi}\frac{\partial}{\partial x}\int\int_A \frac{\rho_x(x',y')\,ds'}{\sqrt{(x-x')^2-(y-y')^2}} = 1 \quad . \tag{5}$$

Integration of (5) then yields

$$\frac{1}{2\pi}\int\int_A \frac{\rho_x(x',y')dx'dy'}{\sqrt{(x-x')^2+(y-y')^2)}} = x \quad . \tag{6}$$

Using the additional constaint on ρ_x defined by (4), it can be shown that the integration constant is zero.

Equation (6) has been solved by the Method of Moments using the following procedure. First, $\rho_x(x',y')$ is expanded using two dimensional pulse functions, $f_n(x',y')$, as follows

$$\rho_x(x',y') = \sum_{n=1}^{N} \alpha_n f_n(x',y') \tag{7}$$

where $f_n = 1$ *on* ΔS_n and equals zero elsewhere.

Substituting (6) into (5)leads to the following set of equations

$$\sum_{n=1}^{N}\int\int_A f_n(x',y')\ k(x,y|x',y')dx'dy' = \sum_{n=1}^{N}\alpha_n \int_{x_n-\Delta x}^{x_n+\Delta x}\int_{y_n-\Delta y}^{y_n+\Delta y} k(x,y|x',y')dx'dy' = x \quad . \tag{8}$$

By using delta functions for testing or applying colocation, the following system of equations is obtained

$$\sum_{n=1}^{N} \alpha_n K_{mn} = x_m \tag{9}$$

where

$$K_{mn} = \int_{x_n-\Delta x}^{x_n+\Delta x} \int_{y_n-\Delta y}^{y_n+\Delta y} k(x_m, y_m | x', y') dx' dy' \ . \tag{10}$$

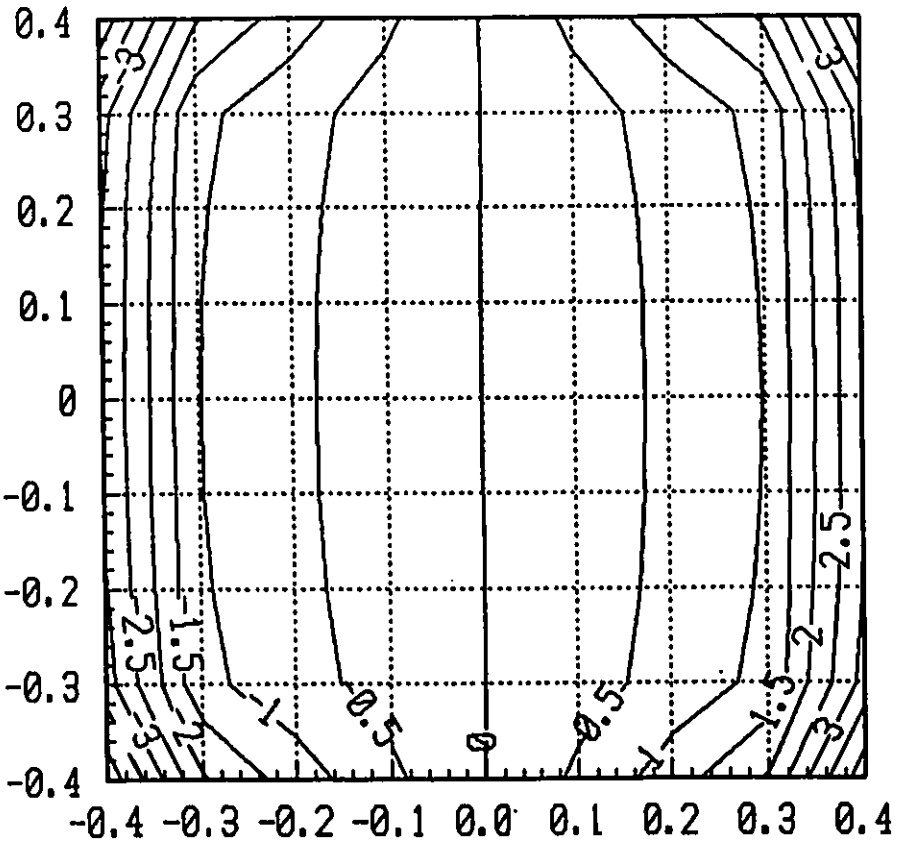

Figure 1 - Variation of ρ_s in a Square Aperture

Using the approximations for K_{mn} given in Appendix 1, a computer program was written to solve this system of linear equations. Figure 1 shows the results for ρ_x using 11 segments.

These results are in agreement with those of de Meulenaere and van Bladel [22] for other aperture shapes as shown below in Figure 2. The results of de Meulenaere and van Bladel are thought to have been calculated using a finite difference method.

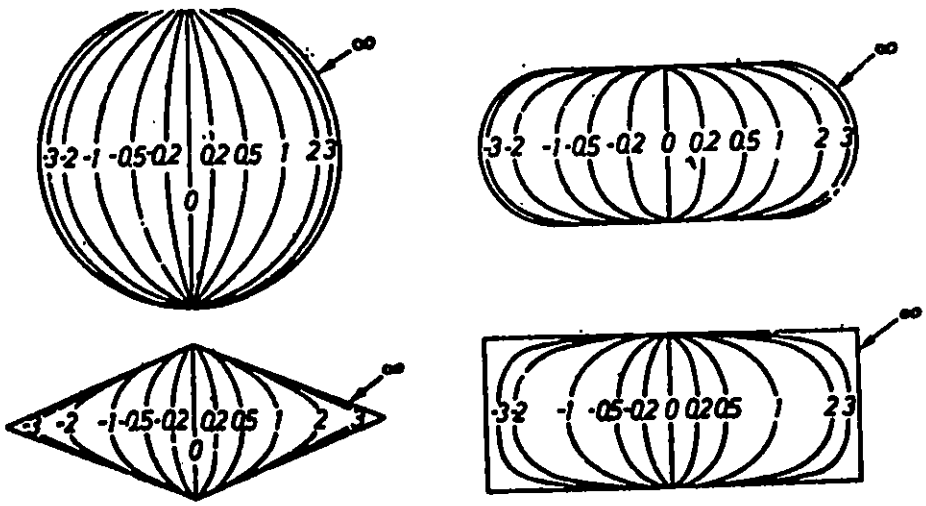

Figure 2 - Variation of ρ_x for some Aperture Cross Sections [22]

Appendix 3

```
c       Description
c       -----------
c       This program calculates the irrotational component of the
c       magnetic surface current for a small square aperture that
c       is open or loaded with an isotropic resistive sheet. The
c       aperture is located in a perfectly conducting screen of
c       infinite extent. The equations have been solved using the
c       Method of Moments.
c
c       The Moment Method matrix equation to be solved has the form
c
c                                        S_mn V_n = B_m
c
C       28 APRIL 1992
C
        COMPLEX V(180), S(180,180), B(180),wv(180)
        complex sum_mx, sum_my, u, ds
        integer pivot(200)
        dimension xreal(90), ximag(90), yreal(90), yimag(90)
        OPEN(UNIT=1, FILE='IRROT_MS', STATUS='NEW')
C
C       Input Data
C
        TYPE 101
101     FORMAT(' NO. OF SEGMENTS= ')
        ACCEPT 102, MA
102     FORMAT(I4)
        M=MA-1
        type*, ' Input Frequency(MHz)'
        accept 104, freq
        type*, ' Input Aperture Size (cm)'
        accept 104, ax
        type*, 'Input Conductivity(mho-cm)'
        accept 104,cond
        wlgth = 3.e+04/freq
        dx=ax/m                                  !Normalization factor
        wlgth_norm = wlgth/dx
        cond_norm = cond*dx
        eta = 377.
        pi = 3.1416
        coef = 8.*eta*(pi**2)
        U=(0.,1.)
```

```
      ds=U*(coef/wlgth_norm)*(cond_norm/2.)
C
C     Construct Moment Method Matrix - M_s^x
C
      LL=M*(M-1)
      II=0
      DO 130 I=2,M
         DO 129 J=2,M+1
            II=II+1
            JJ=0
            DO 128 K=2,M
               DO 127 L=2,M+1
                  JJ=JJ+1
                  IA=K-I-1
                  JA=L-J
                  CALL KERNEL(IA,JA,G1)
                  IA=K-I+1
                  CALL KERNEL(IA,JA,G2)
                  IA=K-I
                  JA=L-J
                  CALL KERNEL(IA,JA,G5)
                  IA=K-I-1
                  JA=L-J-1
                  CALL KERNEL(IA,JA,G6)
                  IA=K-I+1
                  JA=L-J+1
                  CALL KERNEL(IA,JA,G7)
                  IA=K-I+1
                  JA=L-J-1
                  CALL KERNEL(IA,JA,G8)
                  IA=K-I-1
                  JA=L-J+1
                  CALL KERNEL(IA,JA,G9)
                  S(II,JJ)=G1+G2-(2.*G5)
                  S(II+LL,JJ)=(G7-G8-G9+G6)/4.
  127          CONTINUE
  128       CONTINUE
  129    CONTINUE
  130 CONTINUE
```

```
c
c          Construct Moment Method Matrix - M_s^y
c
           II=0
           DO 230 I=2,M
              DO 229 J=2,M+1
                 II=II+1
                 JJ=0
                 DO 228 K=2,M
                    DO 227 L=2,M+1
                      JJ=JJ+1
                      IA=K-I
                      JA=L-J-1
                      CALL KERNEL(IA,JA,G3)
                      JA=L-J+1
                      CALL KERNEL(IA,JA,G4)
                      JA=L-J
                      CALL KERNEL(IA,JA,G5)
                      IA=K-I-1
                      JA=L-J-1
                      CALL KERNEL(IA,JA,G6)
                      IA=K-I+1
                      JA=L-J+1
                      CALL KERNEL(IA,JA,G7)
                      IA=K-I+1
                      JA=L-J-1
                      CALL KERNEL(IA,JA,G8)
                      IA=K-I-1
                      JA=L-J+1
                      CALL KERNEL(IA,JA,G9)
                      S(II,JJ+LL)=(G7-G8-G9+G6)/4.
                      S(II+LL,JJ+LL)=G3+G4-(2.*G5)
227                CONTINUE
228              CONTINUE
229           CONTINUE
230        CONTINUE
c
c
           N=2.*(M-1)*M
           NA=N/2
           LB=2*LL
```

```
c
c       Modify Diagonal Elements of S for Loaded Aperture
c
        do i=1,n
          s(i,i) = s(i,i) + ds
        enddo
c
c       Construct B-Vector
c
        DO 2 I=1,NA
        B(I)=-U*(COEF/WLGTH_NORM)
        B(I+LL)=0.0
2       CONTINUE
C
C       CALL LINPACK MATRIX ROUTINES TO SOLVE PROBLEM
C
        call cLU_Factors_co(S,180,N,pivot,Rcond1,wv)
        if(info.ne.1) then
          write(1,*) ' info=',info
          stop
        endif
        call Cgesl(S,180,N,pivot,B,V)
        write(1,130) Rcond1
130     format(' The recip. cond. num. was ',e9.2)
C
C       Output Data
C
        write(1,106)
106     format('      ')
        write(1,107) freq
107     format(' Frequency = ',f10.4,' MHz')
        write(1,108) ax
108     format(' Aperture Size = ',f10.4,' cm')
        write(1,55) cond
55      format(' Conductivity = ',e10.4,' mho-cm')
        j=0
        sumxr=0.
        sumxi=0.
        do i=1,na
          j=j+1
          xreal(j)=real(v(i))
          ximag(j)=aimag(v(i))
          sumxr=sumxr+xreal(j)
          sumxi=sumxi+ximag(j)
```

```
      enddo
      j=0
      sumyr=0.
      sumyi=0.
      do i=na+1,na+n
        j=j+1
        yreal(j)=real(v(i))
        yimag(j)=aimag(v(i))
        sumyr=sumyr+yreal(j)
        sumyi=sumyi+yimag(j)
      enddo
      nn=1
      write(1,46)
46    format(/,' real Mx')
      lx=m
      ly=m-1
      do i=1,ly
        write(1,112) (xreal(j),j=nn,nn+lx-1)
112     format(9E12.4)
        nn=nn+lx
      enddo
      write(1,50) sumxr
50    format(' sumxr=',e12.4)
      nn=1
      write(1,47)
47    format(/,' imag Mx',/)
      do i=1,ly
        write(1,112) (ximag(j),j=nn,nn+lx-1)
        nn=nn+lx
      enddo
      write(1,51) sumxi
51    format(' sumxi=',e12.4)
      nn=1
      write(1,48)
48    format(/,' real My')
      do i=1,ly
        write(1,112) (yreal(j),j=nn,nn+lx-1)
        nn=nn+lx
      enddo
      write(1,52) sumyr
52    format(' sumyr=',e12.4)
      nn=1
      write(1,49)
49    format(/,' imag My')
```

```
      do i=1,iy
        write(1,112) (yimag(j),j=nn,nn+lx-1)
        nn=nn+lx
      enddo
      write(1,53) sumyi
53    format(' sumyi=',e12.4)
      STOP
      END

C
C     SUBROUTINE KERNEL
C
c     Evaiuation of Integrals Using the Relationship
c
c     ∫∫ dxdy/r = xlog(y+r) + ylog(x+r)
c
      SUBROUTINE KERNEL(IA,JA,G)
      XU=IA+0.5
      XL=IA-0.5
      YU=JA+0.5
      YL=JA-0.5
      XU2=XU*XU
      XL2=XL*XL
      YU2=YU*YU
      YL2=YL*YL
      R5=XL2+YL2
      R6=XU2+YL2
      R7=XL2+YU2
      R8=XU2+YU2
      R1=SQRT(R5)
      R2=SQRT(R6)
      R3=SQRT(R7)
      R4=SQRT(R8)
      AYL=YL*ALOG((XU+R2)/(XL+R1))
      AYU=YU*ALOG((XU+R4)/(XL+R3))
      AXL=XL*ALOG((YU+R3)/(YL+R1))
      AXU=XU*ALOG((YU+R4)/(YL+R2))
      G=AXU-AXL+AYU-AYL
      RETURN
      END
```

Appendix 4

```
c     Description
c     -----------
c     This program calculates the solenoidal component of the
c     magnetic surface current for a small, square aperture that
c     is open or loaded with an isotropic resistive sheet. The
c     aperture is located in a conductive screen of infinite extent.
c     The equations have been solved using the Method of Moments.
c
c     The Moment Method Matrix to be Solved has the Form
c                  S_mn TAU_n = B_m
C
C     4 May 1992
C
      COMPLEX TAU(90), TAU1(90), S1(90,90), U, WV(90)
      COMPLEX B(90), B1(90), S(90,90),C(90,90), X(90)
      DIMENSION xreal(90), ximag(90), xreal1(90), ximag1(90)
      INTEGER pivot(90)
      OPEN(UNIT=1, FILE='SOL_MS', STATUS='NEW')
C
C     INPUT BASIC DATA
C
      TYPE 101
101   FORMAT(' NO. OF SEGMENTS= ')
      ACCEPT 102, MA
102   FORMAT(I4)
104   FORMAT(F10.4)
      M=MA-1
      type*, ' Input Frequency(MHz)'
      accept 104, freq
      type*,' Input Aperture Size(cm)'
      accept 104, ax
      type*, ' Input Conductivity(mho/cm)'
      accept 104, cond
      wlgth = 3.0e+04/freq
      dx = ax/m                          !Normalization Factor
      wlgth_norm = wlgth/dx
      cond_norm = cond*dx
      eta = 377.
      pi = 3.1416
      u=(0.,1.)
```

```
C
C     CONSTRUCT MOMENT METHOD MATRIX - OPEN APERTURE
C
      II=0
      DO 130 I=2,M
        IB=I-1
        IC=I-((MA+1)/2)
        x(ib) = ic
        B1(IB)=-4.*pi*eta*IC
        DO 129 J=2,M
          II=II+1
          JJ=0
          DO 128 K=2,M
            DO 127 L=2,M
              JJ=JJ+1
50            FORMAT(2I4)
              IA=K-I
              JA=L-J
              ARG=FLOAT(IA**2+JA**2)
              IF(IA.EQ.0.AND.JA.EQ.0) GO TO 32
              G1=1./SQRT(ARG)
              GO TO 41
32            G1=3.54
41            C(K,L)=G1
              S(II,JJ)=C(K,4L)
              s1(ii,jj)=c(k,l)
127         CONTINUE
128       CONTINUE
129     CONTINUE
130   CONTINUE
C
C     CONSTRUCT B-VECTOR
C
      N=(M-1)**2
      ID=0
      DO 60 I=1,N,M-1
        ID=ID+1
        DO 70 J=1,M-1
          K=I+J-1
          B(K)=B1(ID)
70      CONTINUE
60    CONTINUE
```

```
C
C       MODIFY MOMENT METHOD MATRIX FOR LOADED APERTURE
C
        do i=1,n
          s1(i,i)=s1(i,i)-U*wlgth_norm*cond_norm
        enddo
C
C       Call LINPACK Matrix Routines
C
        call cLU_Factors_co(S,90,N,pivot,info,Rcond1,wv)
        if(info.ne.0) then
          write(1,*) ' info=', info
          stop
        endif
        call Cgesl(S,90,N,pivot,B,TAU)
        print*, Rcond1
        call cLU_Factors_co(S1,90,N,pivot,info,Rcond1,wv)
        if(info.ne.0) then
          write(1,*) ' info=', info
          stop
        endif
        call Cgesl(S1,90,N,pivot,B,TAU1)
        print*, Rcond1
C
C       Output Data
C
        LL=MA-2
        NN=1
        j=0
        sumxr=0.0
        sumxi=0.0
        do i=1,n
          j=j+1
          xreal(j)=real(tau(i))
          ximag(j)=aimag(tau(i))
          sumxr=sumxr+xreal(j)
          sumxi=sumxi+ximag(j)
        enddo
        j=0
        sumxr1=0.0
        sumxi1=0.0
        do i=1,n
          j=j+1
          xreal1(j)=real(tau1(i))
```

```
      ximag1(j) = aimag(tau1(i))
      sumxr1 = sumxr1 + xreal1(j)
      sumxi1 = sumxi1 + ximag1(j)
    enddo
    write(1,*),' Real Ms'
    write(1,*) ' '
    nn = 1
    do i = 1,ll
      write(1,112) (xreal(j),j = nn,nn + ll-1)
      nn = nn + ll
    enddo
112 format(9E12.4)
    write(1,*),' Imag. Ms'
    write(1,*) ' '
    nn = 1
    do i = 1,ll
      write(1,112) (ximag(j),j = nn,nn + ll-1)
      nn = nn + ll
    enddo
    write(1,*),' Real Ms1'
    write(1,*) ' '
    nn = 1
    do i = 1,ll
      write(1,112) (xreal1(j),j = nn,nn + ll-1)
      nn = nn + ll
    enddo
    write(1,*),' Imag. Ms1'
    write(1,*) ' '
    nn = 1
    do i = 1,ll
      write(1,112) (ximag1(j),j = nn,nn + ll-1)
      nn = nn + ll
    enddo
    SUM = 0.0
    k = 0
    do i = 1,ll
      do j = 1,ll
        k = k + 1
        sum = sum + x(i)*tau(k)
      enddo
    enddo
```

```
      SUM1 = 0.0
      k = 0
      do i = 1,ll
        do j = 1,ll
          k = k + 1
          sum1 = sum1 + x(i)*tau1(k)
        enddo
      enddo
      WRITE(1,113) sum,sum1
113   FORMAT(' SUM = ',E10.4,' SUM1 = ',E10.4)
      STOP
      END
```